Title

Somatic LINE-1 retrotransposition in cortical neurons and non-brain tissues of Rett patients and healthy individuals

Authors and Affiliations

Boxun Zhao[1,2], Qixi Wu[3,4], Adam Yongxin Ye[4,5,6], Jing Guo[1,7], Xianing Zheng[1,2], Xiaoxu Yang[5], Linlin Yan[5], Qing-Rong Liu[8], Thomas M. Hyde[9,10], Liping Wei[1,2,5,*], August Yue Huang[5,*]

1 National Institute of Biological Sciences, Beijing, 102206, China

2 Graduate School of Peking Union Medical College, Beijing, 100730, China

3 School of Life Sciences, Peking University, Beijing, 100871, China

4 Peking-Tsinghua Center for Life Sciences, Beijing, 100871, China

5 Center for Bioinformatics, State Key Laboratory of Protein and Plant Gene Research, School of Life Sciences, Peking University, Beijing, 100871, China

6 Academy for Advanced Interdisciplinary Studies, Peking University, Beijing, 100871, China

7 College of Life Sciences, Beijing Normal University, Beijing, 100875, China

8 Laboratory of Clinical Investigation, National Institute on Aging, Baltimore, MD 21224, USA

9 Lieber Institute for Brain Development, Baltimore, MD 21205, USA

10 Departments of Psychiatry & Behavioral Sciences and Neurology, Johns Hopkins University School of Medicine, Baltimore, MD 21205, USA

*Correspondence

Correspondence should be addressed to A.Y.H. (huangy@mail.cbi.pku.edu.cn) and L.W. (weilp@mail.cbi.pku.edu.cn).

Short title

Somatic L1 mosaicism in Rett and healthy individuals

Keywords

mosaicism, retrotransposition, somatic insertion, Rett syndrome

Abstract

Mounting evidence supports that LINE-1 (L1) retrotransposition can occur postzygotically in healthy and diseased human tissues, contributing to genomic mosaicism in the brain and other somatic tissues of an individual. However, the genomic distribution of somatic L1Hs (Human-specific LINE-1) insertions and their potential impact on carrier cells remain unclear. Here, using a PCR-based targeted bulk sequencing approach, we profiled 9,181 somatic insertions from 20 postmortem tissues from five Rett patients and their matched healthy controls. We identified and validated somatic L1Hs insertions in both cortical neurons and non-brain tissues. In Rett patients, somatic insertions were significantly depleted in exons—mainly contributed by long genes—than healthy controls, implying that cells carrying *MECP2* mutations might be defenseless against a second exonic L1Hs insertion. We observed a significant increase of somatic L1Hs insertions in the brain compared with non-brain tissues from the same individual. Compared to germline insertions, somatic insertions were less sense-depleted to transcripts, indicating that they underwent weaker selective pressure on the orientation of insertion. Our observations demonstrate that somatic L1Hs insertions contribute to genomic diversity and MECP2 dysfunction alters their genomic patterns in Rett patients.

Author Summary

Human-specific LINE-1 (L1Hs) is the most active autonomous retrotransposon family in the human genome. Mounting evidence supports that L1Hs retrotransposition occurs postzygotically in the human brain cells, contributing to neuronal genomic diversity, but the extent of L1Hs-driven mosaicism in the brain is debated. In this study, we profiled genome-wide L1Hs insertions among 20 postmortem tissues from Rett patients and matched controls. We identified and validated somatic L1Hs insertions in both cortical neurons and non-brain tissues, with a higher jumping activity in the brain. We further found that MECP2 dysfunction might alter the genomic pattern of somatic L1Hs in Rett patients.

Introduction

The term "somatic mosaicism" describes the genomic variations that occur in the somatic cells that make up the body of an individual. These variations contribute to intra-individual genetic diversity among different cells (Campbell et al., 2015). In addition to various types of cancers, somatic mosaicisms reportedly contribute to a variety of neurological disorders, including epilepsy, neurodegeneration, and hemimegalencephaly (Poduri et al., 2013). The human-specific LINE-1 (L1Hs) retrotransposon family is the only known family of active autonomous transposons in the human genome (Hancks and Kazazian, 2012; Kazazian and Moran, 2017). L1s retrotranspose through a process called target-primed reverse transcription (TPRT), with the capacity for *de novo* insertion into new genomic locations in both germline and somatic cells (Cost et al., 2002; Luan et al., 1993). Mounting evidence supports that L1Hs elements, with increased copy number in the brain relative to

other tissues, contribute to neuronal diversity via somatic retrotransposition (Coufal et al., 2009; Erwin et al., 2016; Evrony et al., 2012; Evrony et al., 2015; Muotri et al., 2010; Upton et al., 2015).

Recent studies reported the occurrence of somatic L1Hs insertions during neurogenesis and in non-dividing mature neurons (Coufal et al., 2009; Macia et al., 2017). Other studies have observed dysregulated L1Hs copy number in patients with Rett syndrome (Muotri et al., 2010) and schizophrenia (Bundo et al., 2014). Methyl-CpG binding protein 2 (*MECP2*) is the major disease-causing gene of Rett syndrome (Amir et al., 1999). Its gene product, MeCP2, can bind to the 5' UTR of L1 elements and represses their expression and retrotransposition (Yu et al., 2001). While it is known that L1 expression and copy number are elevated in the brains of *Mecp2* knockout mice as well as in patients with Rett syndrome (Muotri et al., 2010; Skene et al., 2010), little is known about the genomic distribution patterns of somatic L1Hs insertions in Rett patients and healthy individuals.

In contrast to germline insertions, the effects of somatic transposon insertions depend not only on their genomic location. Rather, the specific timing, tissue, and cell lineage at which they occur profoundly influence the impact of somatic insertions (Frank, 2010). Single-cell targeted sequencing approaches have been used to identify somatic insertions (Erwin et al., 2016; Evrony et al., 2012; Upton et al., 2015). However, such methods typically require a large number of cells and demand considerable sequencing depth for unbiased profiling of human tissues (Grun and van Oudenaarden, 2015; Navin, 2015). Furthermore, owing to the rarity of somatic insertions, investigations of the clonal diversity of somatic insertions would require the sequencing of even larger numbers of cells (Navin, 2015).

83 Another limitation of single-cell sequencing approaches is that errors of allelic dropout and locus
84 dropout, which frequently occur during the whole genome amplification (WGA) step of library
85 construction, can reduce the sensitivity and specificity of somatic insertion detection. Estimates of the
86 rate of somatic L1Hs insertions vary widely in single-cell genomics studies (Faulkner and Garcia-
87 Perez, 2017). Bulk sequencing approach can potentially overcome these limitations and enable the
88 genome-wide identification and quantification of somatic L1Hs insertions, but their low allele
89 frequency in cell populations poses a great challenge to distinguishing true insertion events from
90 technical artifacts (Evrony et al., 2016).
91
92 Here, we introduced a PCR-based multiplex bulk sequencing method for sensitive enrichment and
93 specific identification of L1Hs insertions from various types of human tissues. We used this method to
94 perform genome-wide L1Hs insertion profiling of 20 postmortem tissues from five patients with Rett
95 syndrome and their matched healthy controls. The aims of this study were to explore the genomic
96 patterns of somatic L1Hs insertions in neuronal and non-neuronal samples, and to investigate whether
97 MECP2 dysfunction could alter the distribution of L1Hs retrotransposition in patients with Rett
98 syndrome.
99

100 **Results**

101 **A bulk sequencing method to identify L1Hs insertions**

102 Systematic genome-wide profiling of somatic L1Hs insertions requires effective enrichment of

103 insertion signals and specific identification of true signals from background noise. Enriching neuronal
104 nuclei from bulk brain tissue facilitates the accurate deciphering of cell type-specific characteristic and
105 increases the chance of identifying clonal somatic insertions that are derived from the same progenitor
106 cell and shared by multiple neurons. Therefore, we labeled prefrontal cortex (PFC) neuronal nuclei
107 using an antibody against neuron-specific marker NeuN (Mullen et al., 1992), and subsequently
108 purified $NeuN^+$ nuclei from postmortem human PFC by fluorescence-activated cell sorting (FACS)
109 (Fig 1A; S1A–D Fig; Appendix 1). All initially sorted nuclei were re-analyzed with a second round of
110 FACS, and the purity of the initial sorting was found to be > 96% (S1E–F Fig; Appendix 1). The
111 integrity and purity of sorted nuclei were confirmed by fluorescence microscopy (S2A–C Fig).
112
113 To distinguish the signals of active L1Hs elements from other transposon families that are typically
114 inactive in human, we developed a method called human active transposon sequencing (HAT-seq) (Fig
115 1B; S3A Fig; S1 Table) based on ATLAS (Badge et al., 2003) and several versions of high-throughput
116 sequencing-based L1 amplification methods (Erwin et al., 2016; Ewing and Kazazian, 2010; Philippe
117 and Cristofari, 2016; Tang et al., 2017). Firstly, L1Hs insertions were specifically enriched and
118 amplified using a primer targeting the diagnostic "AC" motif of L1Hs (Hancks and Kazazian, 2012;
119 Ovchinnikov et al., 2001). To ameliorate the poor performance of Illumina sequencing platform for
120 low-diversity libraries, we employed a nucleotides-shifting design by adding two, four, or six random
121 nucleotides upstream of the L1Hs-specific primer, which greatly increased the diversity of the
122 structure-transformed semi-amplicon library and markedly improved the sequencing quality of L1Hs
123 3' end. The constructed libraries preserved information regarding the insertion direction and were

124 sequenced by multiplexed 150 bp paired-end reads. This approach provided sequence information fully
125 spanning the 3' L1Hs-genome junction of each of L1Hs insertions, which enabled the identification of
126 integration sites and facilitated *in silico* false-positive filtering based on both sequence features and
127 read-count.
128
129 Genomic position of each L1Hs insertion was determined by the alignment of its 3' flanking sequence
130 (Fig 1C). A custom data analysis pipeline classified putative insertions into one of the following four
131 categories: known reference (KR) germline insertions, known non-reference (KNR) germline
132 insertions, unknown (UNK) germline insertions, and putative somatic insertions (S3B Fig). To further
133 remove technical artifacts induced by non-specific or chimeric amplification and read misalignment
134 in next-generation sequencing, we designed a series of stringent error filters to remove them in
135 different aspects (Table 1): 1) read pairs with non-specific amplification signals and incorrect 3'
136 truncation were removed based on the sequence of L1Hs 3' end (Read 2); 2) after merging paired-end
137 reads into contigs, chimeric molecules with abnormal contig structures were identified by BLAST and
138 filtered out; 3) reads with inconsistencies in BWA-MEM and BLAT alignments were defined as
139 mapping errors; and 4) putative somatic insertion signals without multiple PCR duplicates or those
140 present in different individuals were removed, as they were deemed likely to have resulted from
141 sequencing errors. After applying these error filters, the remaining insertions were annotated with peak
142 features to facilitate downstream analysis.
143

144 **Table 1. Error filters used in the computational pipeline.**

Filter name	Definition
Improper alignment	We rejected reads with less than 30-bp alignment or more than 3 mismatches to the reference genome.
Diagnostic motif	We rejected reads without L1Hs diagnostic G motif (position 6012 relative to the L1Hs Repbase consensus) (Bao et al., 2015).
Chimera within L1 segment	We rejected reads with less than 95% identity (> 4 mismatches) to the L1Hs 3' end consensus sequence.
Chimera within poly-A tail	We rejected reads at risk of being chimeric (Upton et al., 2015). Read was re-aligned to hg19 using BLAST to find the corresponding best alignments for the non-retrotransposon and retrotransposon segments. Read was removed as a putative chimera when the overlap of the two best segments was > 10 bp and A% ≥ 50% or 6–10 bp and A% < 50%.
Subfamily filter	We rejected putative somatic insertion sites that overlapped with L1 young subfamilies (L1Hs and L1PA2–4) reference insertions.
Known non-reference filter	We rejected putative somatic insertion sites that overlapped with known non-reference L1 insertions in eul1db (Mir et al., 2015).
Misaligned reads	We rejected reads at risk of being misaligned, defined as inconsistent BWA and BLAT alignment.
Local SV	We rejected reads at risk of being derived from a nearby reference L1Hs (Upton et al., 2015). We extracted 2 kb from the reference genome extending downstream from an aligned non-retrotransposon section and aligned the full read contig against this region with BLAT to exclude genomic rearrangements.
Observed in common	We rejected putative somatic insertion sites observed in two or more individuals.
PCR duplicate	We rejected somatic insertion sites without supporting PCR duplicates.

145

146 **Performance evaluation of the HAT-seq method using a positive control**

147 To benchmark the performance of HAT-seq for detecting somatic L1Hs insertions, we experimentally
148 generated a series of positive control samples with insertions at different frequencies by mixing the
149 genomic DNA (gDNA) extracted from the blood samples of two unrelated adults, ACC1 and ACC2
150 (see details in Materials and Methods). 172 ACC1 non-reference germline L1Hs insertions were
151 identified by HAT-seq, 64 of which were confirmed to be ACC1-specific by 3' junction PCR (3' PCR)
152 analysis of gDNA from ACC1 and ACC2 (Fig 2A; S2 Table; Appendix 2) and thus served as positive
153 controls. Three HAT-seq libraries were generated from samples consisting of ACC2 gDNA spiked with
154 1%, 0.1%, or 0.01% of ACC1 gDNA. Considering that decreasing the number of cells pooled for
155 sequencing increased the signal-to-noise ratio for detecting somatic insertions (Evrony et al., 2016),
156 each HAT-seq library was constructed from 20 ng input (about 3,000 cells).
157
158 The zygosity of ACC1-specific L1Hs insertions was confirmed by full-length PCR: 49 of which were
159 heterozygous, 9 of which were homozygous, and 6 of which were zygosity-undetermined (Fig 2B; S2
160 Table; Appendix 2). We detected all 64 ACC1-specific insertions in our positive control 1% ACC1
161 spike-in library, 49 (76.6%) of which passed all of error filters and subsequently were deemed
162 "identified" by HAT-seq. In the 0.1% library, we detected 23 ACC1-specific insertions (16
163 heterozygous, 4 homozygous, and 3 zygosity-undetermined), 17 (73.9%) of which were identified. In
164 the 0.01% library, we detected seven heterozygous ACC1-specific insertions, five (71.4%) of which
165 were identified. The distributions of signal counts (reads with unique start positions) per ACC1-
166 specific insertion followed the Poisson distribution (Fig 2C), indicating a similar probability for each

167 of ACC1-specific insertions to be randomly sampled. In the 1%, 0.1%, and 0.01% libraries, each of
168 ACC1-specific insertions was diluted to 30, 3, and 0.3 copies. Theoretically, by Poisson statistics, there
169 would be 64, 60.81, and 16.59 ACC1-specific insertions being sampled and subsequently being used
170 as the input of HAT-seq libraries (see details in Materials and Methods). Therefore, we estimated the
171 sensitivity of HAT-seq for somatic L1Hs insertions in 1%, 0.1%, and 0.01% libraries as 76.6% (49/64),
172 28% (17/60.81), and 30.1% (5/16.59), respectively. Our data showed that, with about 3,000 cells as
173 input, HAT-seq was able to detect somatic insertion events present in a single cell (Fig 2D and
174 Appendix 3).
175
176 To further evaluate the efficacy of our L1Hs identification pipeline, we compared the proportions of
177 true positives and false positives after applying all the error filters. For the most stringent evaluation,
178 only those 64 ACC1-specific germline insertions in spike-in libraries were defined as "true positives";
179 all other signals were defined as "false positives", which might include both background noise and
180 some true somatic insertions present in the blood gDNA. As shown in Fig 2E, in three positive control
181 experiments with 1%, 0.1%, and 0.01% ACC1 gDNA spike-in, 76.56%, 73.91%, and 71.43% of true
182 positives remained after all filters, whereas only 3.40% (66), 6.90% (181), and 7.70% (183) of false
183 positives remained after all filters (S3 Table). These results showed that HAT-seq performed in
184 combination with our error filters could successfully remove most artifacts and identify very low-
185 frequency somatic insertions in bulk DNA samples.
186

187 **Profiling of somatic L1Hs insertions in brain and non-brain human tissues**

188 Next, we applied HAT-seq to 20 bulk samples obtained from postmortem neuronal (PFC neurons) and
189 non-neuronal tissues (heart, eye, or fibroblast) from five Rett syndrome patients and five
190 neurologically normal age-, gender-, and race-matched controls (Table 2 and S4–S7 Table). A total of
191 9,181 putative somatic L1Hs insertions were identified in these 20 HAT-seq libraries (S8 Table). A
192 subset of 137 (1.49%) of these insertions were detected by reads with multiple start positions.
193 Considering that the random fragmentation process in HAT-seq library preparation would result in only
194 one start position shared by all reads generated from a single cell, these 137 insertions should be present
195 in multiple cells in the bulk tissue, and thus classified as "clonal somatic insertions". Based on the
196 performance evaluation of HAT-seq, the lower bound of the precision of overall somatic L1Hs
197 insertions was 60.14%. To demonstrate the validity of these identified somatic insertions *in silico*, we
198 investigated whether they had the hallmark features of TPRT-mediated retrotransposition (see details
199 in Materials and Methods). By exploiting the sequence information of L1 integration junctions, we
200 found that such somatic insertions were significantly enriched in genomic regions containing L1
201 endonuclease cleavage motifs (L1 EN motifs) ($p < 2.2\times10^{-16}$, Wilcoxon rank–sum test; Fig 3A; S4 Fig;
202 S9 Table). Moreover, our identified somatic insertions shared the 25-bp peak of poly-A tail length with
203 the reference L1Hs insertions (Fig 3B and S9 Table), where some of the somatic insertions with shorter
204 tails might be explained by non-TPRT mechanism (Morrish et al., 2002). These features of somatic
205 L1Hs insertions helped to elucidate the specificity of HAT-seq method.

06 **Table 2. Overview of postmortem human tissues.**

UMB ID[a]	Category	Mutation	Age	PMI	Brain tissue	Non-brain tissue	Matched ID	Number of somatic insertions		Rate of somatic insertions per cell		Known reference insertions (KRs)	Known non-reference insertions (KNRs)	Unknown insertions (UNKs)
								Cortical neuron	Non-brain	Cortical neuron	Non-brain			
4882	Rett syndrome	c.763C>T (p.R255X)	17 years 310 days	18 hrs	PFC	Heart	4591	855	364	1.47	1.01	819	194	10
1815	Rett syndrome	IVS3-2 A>G	18 years 130 days	5 hrs	PFC	Eye	1571	589	306	1.30	0.68	806	189	11
4852	Rett syndrome	c.451G>T (p.D151Y)	19 years 280 days	13 hrs	PFC	Eye	1347	380	257	0.89	0.54	824	171	8
4516	Rett syndrome	c.763C>T (p.R255X) [b]	20 years 356 days	9 hrs	PFC	Fibro blast	1846	759	411	1.82	0.69	814	195	7
1420	Rett syndrome	No pathogenic mutations	21 years 22 days	18 hrs	PFC	Heart	1455	708	216	1.31	0.37	824	182	8
4591	Healthy control	NA	16 years 223 days	14 hrs	PFC	Heart	4882	861	190	1.58	0.34	816	187	12
1571	Healthy control	NA	18 years 138 days	8 hrs	PFC	Heart	1815	384	221	0.63	0.57	813	175	11
1347	Healthy control	NA	19 years 76 days	16 hrs	PFC	Heart	4852	553	260	1.08	0.72	806	179	12
1846	Healthy control	NA	20 years 221 days	9 hrs	PFC	Heart	4516	744	296	1.66	0.68	817	175	8
1455	Healthy control	NA	25 years 149 days	7 hrs	PFC	Heart	1420	628	203	1.16	0.41	802	183	11

07 [a] The gender and race for all individuals were female and Caucasian. [b] Genetic variant identified by custom AmpliSeq capture panel (S4 Table).

208 Owing to the rarity of each somatic insertion in the cell population and to the sensitivity limits of
209 various analytical methods, experimental validation of somatic insertions using unamplified bulk DNA,
210 in particular when one of the primers is complementary to numerous homologous sequences in the
211 human genome is very challenging (Appendix 4). In theory, if a somatic insertion was unique to a
212 single cell, it would be impossible to detect it in any replicated gDNA extracted from the same tissue.
213 To circumvent this, we performed single-copy cloning by adapting a modified version of digital nested
214 3' PCR (Evrony et al., 2015) that focused exclusively on clonal somatic insertions with three or more
215 supporting signals, whose mosaicism (percentage of cells) were at least 0.1% based on our
216 experimental design of HAT-seq library (Fig 3C). Five out of eight (62.5%) such clonal insertion sites
217 were confirmed via 3' nested PCR and Sanger sequencing of cloned amplification products (Fig 3D–
218 H and S10 Table). Four of these clonal somatic insertions were located in introns of *TGM6*, *CNTN4*,
219 *DIP2C*, and *DGKB*; three were sense-oriented to transcripts.
220
221 To our knowledge, no somatic insertions in non-brain tissues of healthy individuals has been reported
222 (Faulkner and Billon, 2018). We identified and experimentally validated a heart-specific somatic L1Hs
223 insertion from a healthy individual UMB#1571 (Fig 3D). Leveraging both the 3' and 5' junctions of
224 somatic L1Hs insertions enable us to characterize the terminal site duplications (TSDs) and L1
225 endonuclease cleavage site of insertion. Because most of somatic L1Hs insertions were 5' truncated
226 with varied lengths, we screened and selected 22 high-quality step-wise primers covering the full-
227 length L1Hs elements to capture their 5' junction (Fig 3C; S11 Table; Appendix 4). Using 5' junction
228 nested PCR, we successfully re-captured and Sanger sequenced the 5' junction of the heart-specific
229 L1Hs insertion in the healthy individual (UMB#1571) (Fig 4A and S11 Table). We confirmed this

230 insertion was a full-length somatic L1Hs insertion with 14 bp TSD and a cleavage site at 5'–
231 TT/AAAG–3', similar to the consensus L1 EN motif 5'–TT/AAAA–3' (Fig 4B–D). Notably, we also
232 validated this 5' junction by combining full-length PCR with 5' junction PCR (Fig 4E; see details in
233 Materials and Methods).
234
235 In addition, we verified one fibroblast- and another heart-specific L1Hs insertion in two patients with
236 Rett syndrome (Fig 3E–F). The heart-specific L1Hs insertion in the Rett patient (UMB#1420) was
237 further resolved to be a highly 5' truncated L1Hs insertion (~800 bp) with 9 bp TSD and a cleavage
238 site at 5'–TT/TAAA–3' (S5 Fig and S11 Table). The poly-A tails of these two clonal somatic insertions
239 were experimentally measured to be polymorphic, indicating that they may involve multiple mutations
240 after the original somatic retrotransposition events (Fig 3I and S10 Table). As previously reported
241 (Evrony et al., 2015; Grandi et al., 2013), poly-A tail was shown to be a highly mutable sequence
242 element and might undergo secondary mutations in descendant cells. Furthermore, we confirmed two
243 additional somatic L1Hs insertions from Rett patient UMB#4516 were present in both PFC neurons,
244 PFC glia, and fibroblasts (Fig 3G–H and S6 Fig), suggesting that they might retrotranspose during
245 early embryonic development. Notably, the intronic somatic insertion (chr20:2392172) in *TGM6* was
246 a full-length L1Hs insertion with 15 bp TSD and a cleavage site at 5'–AT/AAAA–3' (S7 Fig and S11
247 Table). We further quantified the allele fractions of this insertion using custom droplet digital PCR
248 (ddPCR) assay and found that 6.34% of fibroblasts and 2.87% of PFC neurons contained this L1Hs
249 insertion (S8A–E Fig and S10 Table). Our observations demonstrated that endogenous L1Hs could
250 retrotranspose in various types of non-brain tissues during human development.
251

252 **Abnormal L1Hs mobilization in patients with Rett syndrome**

253 Our HAT-seq bulk sequencing data enabled us to perform statistical analysis of the exonic and intronic
254 patterns of somatic L1Hs insertions in samples from Rett patients and matched healthy controls. We
255 found 180 somatic insertions that were integrated into exonic regions: 9 of which were located in 5'
256 UTR, 102 of which were located in coding regions, and 69 of which were located in 3' UTR (S12
257 Table). While no significant difference was observed in introns (OR = 0.97, p = 0.44, Fisher's exact
258 test), somatic insertions were significantly depleted in exons (OR = 0.59, $p = 6.6\times10^{-4}$, Fisher's exact
259 test) of Rett patients compared with matched healthy controls (Fig 5A and S13 Table). Previous studies
260 have shown that dysregulation of long genes (> 100 kb) was linked to neurological disorders, including
261 Rett syndrome (Gabel et al., 2015) and autism spectrum disorder (King et al., 2013). We used our HAT-
262 seq data to investigate somatic insertional bias in both long (> 100 kb) and short genes (< 100 kb) of
263 Rett patients. As a result, we found significant depletion of somatic insertions in exons of long genes
264 (OR = 0.27, $p = 5.2\times10^{-5}$, Fisher's exact test) but not short genes (OR = 0.76, p = 0.12, Fisher's exact
265 test; Fig 5B and S13 Table). Our speculation was that if an L1Hs inserted into the exonic regions,
266 especially in important genes, of the *MECP2* mutated cell, the cell would have a higher risk of death
267 and subsequently be cleared up; therefore, the observed exonic depletion of L1 insertions in Rett
268 patients might be resulted from the negative selection acting on those "lethal" exonic insertions.
269
270 In contrast to germline insertions, the impact of somatic insertions depends not only on their genomic
271 location, but also the number of cells carrying that insertion, highlighting the importance of clonal
272 somatic insertions. We found that in cortical neurons of Rett patients, clonal somatic insertions were
273 enriched in introns (OR = 1.85, p = 0.029, Fisher's exact test; Fig 5C and S13 Table); these clonal

274 intronic insertions were significantly enriched in the sense orientation to the transcripts (OR = 3.3, p
275 = 0.0067, Fisher's exact test; Fig 5D and S13 Table). The presence of L1 insertion in the sense
276 orientation has been reported to interfere with transcriptional elongation of co-localized genes (Han et
277 al., 2004). Considering that clonal insertions are more likely to have occurred at an early stage of
278 development and thus affect a relatively large proportion of cells, these distinct insertion pattern in
279 cortical neurons of Rett patients might indicate potential transcriptional burden on the nervous system.
280

281 **Genomic patterns of somatic and germline L1Hs insertions**

282 The design of HAT-seq method allowed for unbiased enrichment of both somatic and germline L1Hs
283 insertions from each of bulk DNA samples. As germline insertion had constant genomic copy number
284 in all tissues from the same donor, we used germline insertion as endogenous control to measure the
285 relative copy number of genome-wide somatic insertions in the brain and non-brain tissues. We
286 quantified the relative somatic L1Hs content by calculating the L1Hs-derived read count ratio of
287 somatic to germline insertions using HAT-seq data of each sample (S14 Table; see details in Materials
288 and Methods). Among all Rett patients and their matched controls, we observed a significant increase
289 in the copy number of somatic L1Hs insertions in PFC neurons relative to matched non-brain tissues
290 (heart, eye, or fibroblast) from the same donor (n = 10, $p = 2.7\times10^{-4}$, paired *t*-test; Fig 6A and S8F–G
291 Fig). We also estimated the occurrence rate of somatic L1Hs insertions based on the germline insertion
292 copy number of each individual (Fig 6B). This produced an average of 1.29 [95% CI: 1.03–1.55]
293 somatic insertions per PFC neuron versus 0.60 [95% CI: 0.46–0.74] insertions per non-brain cell (S14
294 Table). Our observation of higher somatic L1Hs rate in PFC neurons from healthy individuals argued

295 for the active retrotransposition of L1Hs in the human brain (Coufal et al., 2009). One significant
296 advantage of HAT-seq was the ability to distinguish signals of somatic insertions from the
297 overwhelming copies of germline L1Hs insertions in the genome (see details in Materials and
298 Methods). Inconsistent with the previous qPCR result (Muotri et al., 2010), when comparing the group
299 of Rett patients with matched healthy controls, we only observed a slight but not significant increase
300 of somatic L1Hs insertion rate in the Rett group, with 1.36 [range: 0.89–1.82] versus 1.22 [range:
301 0.63–1.66] per PFC neuron and 0.66 [range: 0.37–1.01] versus 0.54 [range: 0.34–0.72] per non-brain
302 cell (Fig 6C and S14 Table).
303
304 We next characterized the genome-wide germline L1Hs insertions. HAT-seq yielded greater than 320-
305 fold enrichment for KR, KNR, and UNK L1Hs insertions (S15 Table). On average, 814 KRs, 183
306 KNRs, and 10 UNKs were identified in each bulk sample (Table 2, S5–7 Table). Hierarchical clustering
307 based on L1Hs profiles correctly paired all neuronal samples with the non-neuronal tissue samples of
308 the same individual (Fig 6D). To experimentally validate the HAT-seq predicted germline insertions,
309 we performed 3' PCR validation on a random subset of polymorphic insertions from among the ten
310 individuals, including 8 sites out of 160 polymorphic KRs, 20 sites out of 451 KNRs, and 2 sites out
311 of 48 UNKs (S7 and S16 Table). As a result, all of the assayed sites were detected in 3' PCR, with
312 98.4% (120/122) and 100% (168/168) sensitivity and specificity, respectively (S16 Table and
313 Appendix 5). These results support that HAT-seq can reliably detect germline L1Hs insertions with
314 high sensitivity and specificity.
315

316 Previous studies have shown that intronic germline L1Hs insertions are sense-depleted (Ewing and
317 Kazazian, 2010; Smit, 1999; Upton et al., 2015). As expected, the germline insertions identified in this
318 study were significantly sense-depleted to the transcripts (633/1,544 [41%], $p = 1.6\times10^{-12}$, binomial
319 test; Fig 6E and S13 Table). It is important to ask the question: whether such orientation bias for
320 germline insertions is resulted from natural selection or insertional preference? To address this, we
321 chose somatic L1Hs insertions as internal reference to control confounding factors. We compared the
322 orientation bias between germline and somatic L1Hs insertions in transcripts and found that germline
323 insertions were significantly sense-depleted than somatic insertions (odds ratio [OR] = 0.79, p =
324 7.9×10^{-4}, Fisher's exact test; Fig 6E and S13 Table). Because somatic L1Hs insertions only affected a
325 small proportion of cells and thus they should undergo weaker selective pressure than germline
326 insertions, our results suggested that natural selection may play a major role in shaping the sense-
327 depleted distribution of germline L1Hs insertions.
328

329 **Discussion**

330 Here, we present HAT-seq, a bulk DNA sequencing method to profile genome-wide L1Hs insertions
331 from physiologically normal and pathological human tissues. We demonstrated that, in addition to
332 neuronal cells (Erwin et al., 2016; Evrony et al., 2012; Evrony et al., 2015; Macia et al., 2017; Upton
333 et al., 2015), L1Hs also retrotransposed in a variety of non-brain tissues and cell types during normal
334 development and contributed to the inter-cellular diversity of the human genome. Using high-
335 throughput sequencing-based quantitative analysis, we found that somatic insertions occurred at a
336 higher rate in brain than in non-brain tissues, consistent with previous studies (Coufal et al., 2009).

337 Previous qPCR and single-cell genomic studies have resulted in conflicting estimates of the frequency
338 of somatic insertions in neurons: ~80 L1 insertions per neuron (Coufal et al., 2009), < 0.04–0.6 L1
339 insertions per neuron (Evrony et al., 2012), 13.7 L1 insertions per neuron (Upton et al., 2015), or
340 ~0.58–1 somatic L1-associated variants per neuron (Erwin et al., 2016). Differential estimates might
341 result from differences in WGA and signal enrichment methods. Using a bulk DNA sequencing
342 approach, we estimated the rate of somatic insertions to be 0.63–1.66 L1Hs insertions per PFC neuron
343 in healthy individuals (Fig 6B and S14 Table).
344
345 Clonally distributed insertions are prevalent in normal brain (Evrony et al., 2015). Increasing evidence
346 suggests that neuronal L1s retrotransposition contributes to the susceptibility to and pathophysiology
347 of neurological disorders, including Rett syndrome (Muotri et al., 2010), schizophrenia (Bundo et al.,
348 2014) and Alzheimer's disease (Guo et al., 2018). We observed that, in PFC neurons of Rett patients,
349 clonal somatic insertions were enriched in introns, and these clonal intronic insertions were
350 significantly enriched in the sense orientation (Fig 5C–D). In particular, in Rett patient UMB#4516,
351 we found a full-length, sense-orientated, intronic somatic insertion (chr20:2392172) in *TGM6* (S7 Fig
352 and S11 Table), a gene associated with central nervous system development and motor function
353 (Thomas et al., 2013), which could potentially dysregulate gene expression (Han et al., 2004). We
354 found that 6.34% of fibroblasts and 2.87% of PFC neurons contained this insertion (S8A–E Fig and
355 S10 Table), suggesting that it might occur in the 16-cell or 32-cell stages during morula stage.
356 Mutations in *TGM6* are associated with spinocerebellar ataxia type 35, one of a group of genetic
357 disorders characterized by poor coordination of hands, gait, speech, and eye movements as well as
358 frequent atrophy of the cerebellum (Guo et al., 2014; Li et al., 2013; Wang et al., 2010). According to

359 the clinical records, UMB#4516 had slight cerebral atrophy and cerebellar degeneration, could not
360 hold things in her hands, and her speech development ceased at 16 months of age; these phenotypes
361 were absent in the other four patients with Rett syndrome. Taken together, our data indicated that this
362 clonal L1Hs insertion of *TGM6* might be correlated with the distinct clinical phenotype of UMB#4516.
363
364 Previous studies have provided evidence for significant selection against older L1 elements that are
365 non-polymorphic (Boissinot et al., 2001; Ewing and Kazazian, 2010). To characterize the insertion
366 pattern of L1 with minimal influence from selective pressure, experimental methods were developed
367 for recovery of novel L1 insertions in cultured cells (Gilbert et al., 2005; Symer et al., 2002). Using
368 HAT-seq method, we were able to distinguish somatic L1Hs insertions from germline L1Hs insertions
369 within the same individual. To determine whether the sense-depleted germline insertion was resulted
370 from natural selection or insertional preference, we used somatic insertion as internal reference to
371 control confounding factors such as intrinsic insertion preference and compared germline with somatic
372 insertions. Our results suggested that natural selection shaped a sense-depleted distribution of germline
373 L1Hs insertions in the human genome.
374
375 Several PCR-based bulk sequencing methods, such as ATLAS (Badge et al., 2003), L1-seq (Ewing
376 and Kazazian, 2010), TIP-seq (Tang et al., 2017), bulk SLAV-seq (Erwin et al., 2016), and ATLAS-seq
377 (Philippe and Cristofari, 2016), have been developed to identify germline L1Hs insertions.
378 Furthermore, L1-seq and TIP-seq have been successfully used in the identification of somatic
379 insertions in tumors (Achanta et al., 2016; Doucet-O'Hare et al., 2015; Ewing et al., 2015; Solyom et
380 al., 2012; Tang et al., 2017). Due to clonal expansion during tumorigenesis, such insertions could affect

381 numerous cells in tumors. To our knowledge, HAT-seq is the first PCR-based bulk sequencing method
382 to identify rare somatic insertions in a subset of cells—even unique cells—in non-tumor tissues. HAT-
383 seq provides not only the genomic positions of somatic insertions but also the allele fraction of each
384 insertion, which is informative for inferring the timing when the insertion has occurred. The
385 sensitivities of HAT-seq for low-frequency somatic L1Hs insertions were relatively low (~30% for
386 insertions present in < 1% fraction of cells). One possible explanation was that some signals of
387 insertion were lost during library construction and NGS sequencing, e.g. sonic fragmentation, clean-
388 ups, size selection, and loading library to sequencer. Single-cell whole genome and targeted sequencing
389 approaches have been used to identify both TPRT-mediated and endonuclease-independent insertions
390 (Erwin et al., 2016; Evrony et al., 2012; Evrony et al., 2015; Upton et al., 2015), where the signal of
391 somatic insertions can be as high as germline heterozygous insertions in single-cell level. However,
392 such single-cell approaches cannot achieve increased sensitivity without cost (Evrony et al., 2016).
393 For example, to detect a given insertion with 0.1% mosaicism, more than 1,000 single cells may need
394 to be amplified and sequenced. Therefore, compared with single-cell approaches, HAT-seq was eligible
395 to identify a large number of somatic L1Hs insertions in a more cost-effective way.
396
397 Based on our experimental design, assembling overlapped read pairs into contigs can provide sequence
398 information fully spanning the L1Hs integration sites, enabling downstream false-positive filtering
399 based on both sequence features and read-count. However, a portion of read pairs were unable to be
400 merged into contigs because the inaccurate size-selection during library construction. Applying the
401 same filtering strategy, we re-analyzed these unassembled read pairs and revealed 11 clonal insertion
402 candidates. Further PCR experiments only validate one of these candidates (9%, S10 Table). Because

403 the key filter "chimera within poly-A tail" was not applicable for unassembled read pairs, our sequence
404 analysis suggested that chimeric molecules bridging within the poly-A tail was the major source of
405 false-positives for unassembled data (see details in Materials and Methods). As shown in the statistics
406 of positive control libraries (S2 Table) and experimental validation, the unassembled data could
407 provide additional signals of somatic L1Hs insertions but require careful analysis and rigorous
408 validation to address technical artifacts. Further gains in statistical power will be benefited from
409 increased sample size and improved efficiency of HAT-seq.

410

411 Several unresolved technical challenges might constrain the total number of detectable L1Hs insertions
412 by the current version of HAT-seq, including the identification of insertions in repetitive regions with
413 low mappability (such as pre-existing L1 germline insertions) and 3' truncated insertions. With rapid
414 innovations in sequencing technology, higher throughput and longer read length will markedly
415 improve the performance of HAT-seq. Future studies that profile all active retrotransposons (i.e., L1Hs,
416 Alu, and SVA) in a variety of cell types, tissues, and developmental stages will shed new light on the
417 dynamics of somatic retrotransposition under host regulation and help to uncover their roles in human
418 disease.

419

420 **Acknowledgements**

421 We acknowledge the UMB Brain and Tissue Bank (University of Maryland, Baltimore, MD) and the
422 Lieber Institute for Brain Development (Baltimore, MD) for providing postmortem human tissues. We
423 are grateful to Drs Eunjung Alice Lee, Daniel R. Weinberger, Li-Lin Du, Meng-Qiu Dong, Yu Zhang,

Ge Gao, Louis Tao, Cheng Li, Jian Lu, and Manyuan Long for their insightful comments and suggestions. We thank Drs Kazuya Iwamoto and Miki Bundo for providing detailed protocols of nuclei isolation. We thank Dr. Timothy W. Yu for providing experimental resources in the revision. We thank the reviewers for constructive feedback on the manuscript. This study was supported by the National Natural Science Foundation of China (31530092) and the Ministry of Science and Technology 863 Grant (2015AA020108). Q-R.L. was supported in part by the Intramural Research Program at the National Institute on Aging.

Author contributions

Adam Yongxin Ye

Formal analysis, Methodology, Visualization, Writing-original draft

August Yue Huang

Conceptualization, Resources, Supervision, Writing—review and editing

Boxun Zhao

Conceptualization, Data curation, Formal analysis, Investigation, Methodology, Project administration, Validation, Visualization, Writing—original draft, Writing—review and editing

Jing Guo

Data curation, Methodology, Validation

Liping Wei

Conceptualization, Funding acquisition, Resources, Supervision, Writing—review and editing

Linlin Yan

Formal analysis

Thomas M. Hyde

Resources

Qing-Rong Liu

Methodology

Qixi Wu

Conceptualization, Investigation, Methodology, Writing—review and editing

Xianing Zheng

Methodology

Xiaoxu Yang

Validation, Visualization

467 **Competing interests**

468 No conflicts of interest.

469 **References**

470 Achanta, P., Steranka, J.P., Tang, Z., Rodic, N., Sharma, R., Yang, W.R., Ma, S., Grivainis, M., Huang,
471 C.R.L., Schneider, A.M., *et al.* (2016). Somatic retrotransposition is infrequent in glioblastomas. Mob
472 DNA *7*, 22.

473 Amir, R.E., Van den Veyver, I.B., Wan, M., Tran, C.Q., Francke, U., and Zoghbi, H.Y. (1999). Rett
474 syndrome is caused by mutations in X-linked MECP2, encoding methyl-CpG-binding protein 2. Nat
475 Genet *23*, 185-188.

476 Badge, R.M., Alisch, R.S., and Moran, J.V. (2003). ATLAS: a system to selectively identify human-
477 specific L1 insertions. Am J Hum Genet *72*, 823-838.

478 Bao, W., Kojima, K.K., and Kohany, O. (2015). Repbase Update, a database of repetitive elements in
479 eukaryotic genomes. Mob DNA *6*, 11.

480 Boissinot, S., Entezam, A., and Furano, A.V. (2001). Selection against deleterious LINE-1-containing
481 loci in the human lineage. Mol Biol Evol *18*, 926-935.

482 Bundo, M., Toyoshima, M., Okada, Y., Akamatsu, W., Ueda, J., Nemoto-Miyauchi, T., Sunaga, F.,
483 Toritsuka, M., Ikawa, D., Kakita, A., *et al.* (2014). Increased l1 retrotransposition in the neuronal
484 genome in schizophrenia. Neuron *81*, 306-313.

485 Campbell, I.M., Shaw, C.A., Stankiewicz, P., and Lupski, J.R. (2015). Somatic mosaicism:
486 implications for disease and transmission genetics. Trends Genet *31*, 382-392.

487 Cost, G.J., Feng, Q., Jacquier, A., and Boeke, J.D. (2002). Human L1 element target-primed reverse
488 transcription in vitro. EMBO J *21*, 5899-5910.

489 Coufal, N.G., Garcia-Perez, J.L., Peng, G.E., Yeo, G.W., Mu, Y., Lovci, M.T., Morell, M., O'Shea, K.S.,
490 Moran, J.V., and Gage, F.H. (2009). L1 retrotransposition in human neural progenitor cells. Nature
491 *460*, 1127-1131.

492 Doucet-O'Hare, T.T., Rodic, N., Sharma, R., Darbari, I., Abril, G., Choi, J.A., Young Ahn, J., Cheng,
493 Y., Anders, R.A., Burns, K.H., *et al.* (2015). LINE-1 expression and retrotransposition in Barrett's
494 esophagus and esophageal carcinoma. Proc Natl Acad Sci U S A *112*, E4894-4900.

Erwin, J.A., Marchetto, M.C., and Gage, F.H. (2014). Mobile DNA elements in the generation of diversity and complexity in the brain. Nat Rev Neurosci *15*, 497-506.

Erwin, J.A., Paquola, A.C., Singer, T., Gallina, I., Novotny, M., Quayle, C., Bedrosian, T.A., Alves, F.I., Butcher, C.R., Herdy, J.R.*, et al.* (2016). L1-associated genomic regions are deleted in somatic cells of the healthy human brain. Nat Neurosci *19*, 1583-1591.

Evrony, G.D., Cai, X., Lee, E., Hills, L.B., Elhosary, P.C., Lehmann, H.S., Parker, J.J., Atabay, K.D., Gilmore, E.C., Poduri, A.*, et al.* (2012). Single-neuron sequencing analysis of L1 retrotransposition and somatic mutation in the human brain. Cell *151*, 483-496.

Evrony, G.D., Lee, E., Mehta, B.K., Benjamini, Y., Johnson, R.M., Cai, X., Yang, L., Haseley, P., Lehmann, H.S., Park, P.J.*, et al.* (2015). Cell lineage analysis in human brain using endogenous retroelements. Neuron *85*, 49-59.

Evrony, G.D., Lee, E., Park, P.J., and Walsh, C.A. (2016). Resolving rates of mutation in the brain using single-neuron genomics. Elife *5*.

Ewing, A.D., Gacita, A., Wood, L.D., Ma, F., Xing, D., Kim, M.S., Manda, S.S., Abril, G., Pereira, G., Makohon-Moore, A.*, et al.* (2015). Widespread somatic L1 retrotransposition occurs early during gastrointestinal cancer evolution. Genome Res *25*, 1536-1545.

Ewing, A.D., and Kazazian, H.H., Jr. (2010). High-throughput sequencing reveals extensive variation in human-specific L1 content in individual human genomes. Genome Res *20*, 1262-1270.

Faulkner, G.J., and Billon, V. (2018). L1 retrotransposition in the soma: a field jumping ahead. Mobile DNA *9*, 22.

Faulkner, G.J., and Garcia-Perez, J.L. (2017). L1 Mosaicism in Mammals: Extent, Effects, and Evolution. Trends Genet *33*, 802-816.

Frank, S.A. (2010). Evolution in health and medicine Sackler colloquium: Somatic evolutionary genomics: mutations during development cause highly variable genetic mosaicism with risk of cancer and neurodegeneration. Proc Natl Acad Sci U S A *107 Suppl 1*, 1725-1730.

Gabel, H.W., Kinde, B., Stroud, H., Gilbert, C.S., Harmin, D.A., Kastan, N.R., Hemberg, M., Ebert, D.H., and Greenberg, M.E. (2015). Disruption of DNA-methylation-dependent long gene repression in Rett syndrome. Nature *522*, 89-93.

Gilbert, N., Lutz, S., Morrish, T.A., and Moran, J.V. (2005). Multiple fates of L1 retrotransposition

524 intermediates in cultured human cells. Mol Cell Biol *25*, 7780-7795.
525 Goodier, J.L. (2014). Retrotransposition in tumors and brains. Mob DNA *5*, 11.
526 Grandi, F.C., Rosser, J.M., and An, W. (2013). LINE-1-derived poly(A) microsatellites undergo rapid
527 shortening and create somatic and germline mosaicism in mice. Mol Biol Evol *30*, 503-512.
528 Grun, D., and van Oudenaarden, A. (2015). Design and Analysis of Single-Cell Sequencing
529 Experiments. Cell *163*, 799-810.
530 Guo, C., Jeong, H.-H., Hsieh, Y.-C., Klein, H.-U., Bennett, D.A., Jager, P.L., Liu, Z., and Shulman,
531 J.M. (2018). Tau Activates Transposable Elements in Alzheimer's Disease. Cell reports *23*, 2874-2880.
532 Guo, Y.C., Lin, J.J., Liao, Y.C., Tsai, P.C., Lee, Y.C., and Soong, B.W. (2014). Spinocerebellar ataxia
533 35: novel mutations in TGM6 with clinical and genetic characterization. Neurology *83*, 1554-1561.
534 Han, J.S., Szak, S.T., and Boeke, J.D. (2004). Transcriptional disruption by the L1 retrotransposon and
535 implications for mammalian transcriptomes. Nature *429*, 268-274.
536 Hancks, D.C., and Kazazian, H.H., Jr. (2012). Active human retrotransposons: variation and disease.
537 Curr Opin Genet Dev *22*, 191-203.
538 Jurka, J. (1997). Sequence patterns indicate an enzymatic involvement in integration of mammalian
539 retroposons. Proc Natl Acad Sci U S A *94*, 1872-1877.
540 Kazazian, H.H., Jr., and Moran, J.V. (2017). Mobile DNA in Health and Disease. N Engl J Med *377*,
541 361-370.
542 King, I.F., Yandava, C.N., Mabb, A.M., Hsiao, J.S., Huang, H.S., Pearson, B.L., Calabrese, J.M.,
543 Starmer, J., Parker, J.S., Magnuson, T.*, et al.* (2013). Topoisomerases facilitate transcription of long
544 genes linked to autism. Nature *501*, 58-62.
545 Li, M., Pang, S.Y., Song, Y., Kung, M.H., Ho, S.L., and Sham, P.C. (2013). Whole exome sequencing
546 identifies a novel mutation in the transglutaminase 6 gene for spinocerebellar ataxia in a Chinese family.
547 Clin Genet *83*, 269-273.
548 Luan, D.D., Korman, M.H., Jakubczak, J.L., and Eickbush, T.H. (1993). Reverse transcription of
549 R2Bm RNA is primed by a nick at the chromosomal target site: a mechanism for non-LTR
550 retrotransposition. Cell *72*, 595-605.
551 Macia, A., Widmann, T.J., Heras, S.R., Ayllon, V., Sanchez, L., Benkaddour-Boumzaouad, M., Munoz-
552 Lopez, M., Rubio, A., Amador-Cubero, S., Blanco-Jimenez, E.*, et al.* (2017). Engineered LINE-1

553 retrotransposition in nondividing human neurons. Genome Res *27*, 335-348.
554 Mir, A.A., Philippe, C., and Cristofari, G. (2015). euL1db: the European database of L1HS
555 retrotransposon insertions in humans. Nucleic Acids Res *43*, D43-47.
556 Morrish, T.A., Gilbert, N., Myers, J.S., Vincent, B.J., Stamato, T.D., Taccioli, G.E., Batzer, M.A., and
557 Moran, J.V. (2002). DNA repair mediated by endonuclease-independent LINE-1 retrotransposition.
558 Nat Genet *31*, 159-165.
559 Mullen, R.J., Buck, C.R., and Smith, A.M. (1992). NeuN, a neuronal specific nuclear protein in
560 vertebrates. Development *116*, 201-211.
561 Muotri, A.R., Marchetto, M.C., Coufal, N.G., Oefner, R., Yeo, G., Nakashima, K., and Gage, F.H.
562 (2010). L1 retrotransposition in neurons is modulated by MeCP2. Nature *468*, 443-446.
563 Navin, N.E. (2015). The first five years of single-cell cancer genomics and beyond. Genome Res *25*,
564 1499-1507.
565 Ovchinnikov, I., Troxel, A.B., and Swergold, G.D. (2001). Genomic characterization of recent human
566 LINE-1 insertions: evidence supporting random insertion. Genome Res *11*, 2050-2058.
567 Philippe, C., and Cristofari, G. (2016). Activation of individual L1 retrotransposon instances is
568 restricted to cell-type dependent permissive loci. eLife.
569 Poduri, A., Evrony, G.D., Cai, X., and Walsh, C.A. (2013). Somatic mutation, genomic variation, and
570 neurological disease. Science *341*, 1237758.
571 Reilly, M.T., Faulkner, G.J., Dubnau, J., Ponomarev, I., and Gage, F.H. (2013). The role of transposable
572 elements in health and diseases of the central nervous system. J Neurosci *33*, 17577-17586.
573 Skene, P.J., Illingworth, R.S., Webb, S., Kerr, A.R., James, K.D., Turner, D.J., Andrews, R., and Bird,
574 A.P. (2010). Neuronal MeCP2 is expressed at near histone-octamer levels and globally alters the
575 chromatin state. Mol Cell *37*, 457-468.
576 Smit, A.F. (1999). Interspersed repeats and other mementos of transposable elements in mammalian
577 genomes. Curr Opin Genet Dev *9*, 657-663.
578 Solyom, S., Ewing, A.D., Rahrmann, E.P., Doucet, T., Nelson, H.H., Burns, M.B., Harris, R.S., Sigmon,
579 D.F., Casella, A., Erlanger, B.*, et al.* (2012). Extensive somatic L1 retrotransposition in colorectal
580 tumors. Genome Res *22*, 2328-2338.
581 Symer, D.E., Connelly, C., Szak, S.T., Caputo, E.M., Cost, G.J., Parmigiani, G., and Boeke, J.D. (2002).

Human l1 retrotransposition is associated with genetic instability in vivo. Cell *110*, 327-338.

Tang, Z., Steranka, J.P., Ma, S., Grivainis, M., Rodic, N., Huang, C.R., Shih, I.M., Wang, T.L., Boeke, J.D., Fenyo, D.*, et al.* (2017). Human transposon insertion profiling: Analysis, visualization and identification of somatic LINE-1 insertions in ovarian cancer. Proc Natl Acad Sci U S A *114*, E733-E740.

Thomas, H., Beck, K., Adamczyk, M., Aeschlimann, P., Langley, M., Oita, R.C., Thiebach, L., Hils, M., and Aeschlimann, D. (2013). Transglutaminase 6: a protein associated with central nervous system development and motor function. Amino Acids *44*, 161-177.

Upton, K.R., Gerhardt, D.J., Jesuadian, J.S., Richardson, S.R., Sanchez-Luque, F.J., Bodea, G.O., Ewing, A.D., Salvador-Palomeque, C., van der Knaap, M.S., Brennan, P.M.*, et al.* (2015). Ubiquitous L1 mosaicism in hippocampal neurons. Cell *161*, 228-239.

Wang, J.L., Yang, X., Xia, K., Hu, Z.M., Weng, L., Jin, X., Jiang, H., Zhang, P., Shen, L., Guo, J.F.*, et al.* (2010). TGM6 identified as a novel causative gene of spinocerebellar ataxias using exome sequencing. Brain *133*, 3510-3518.

Yu, F., Zingler, N., Schumann, G.G., and Stratling, W.H. (2001). Mecp2 represses L1 expression and retrotransposition but not Alu transcription. Nucleic Acids Res *29*, 4493-4501.

599 **Figures**

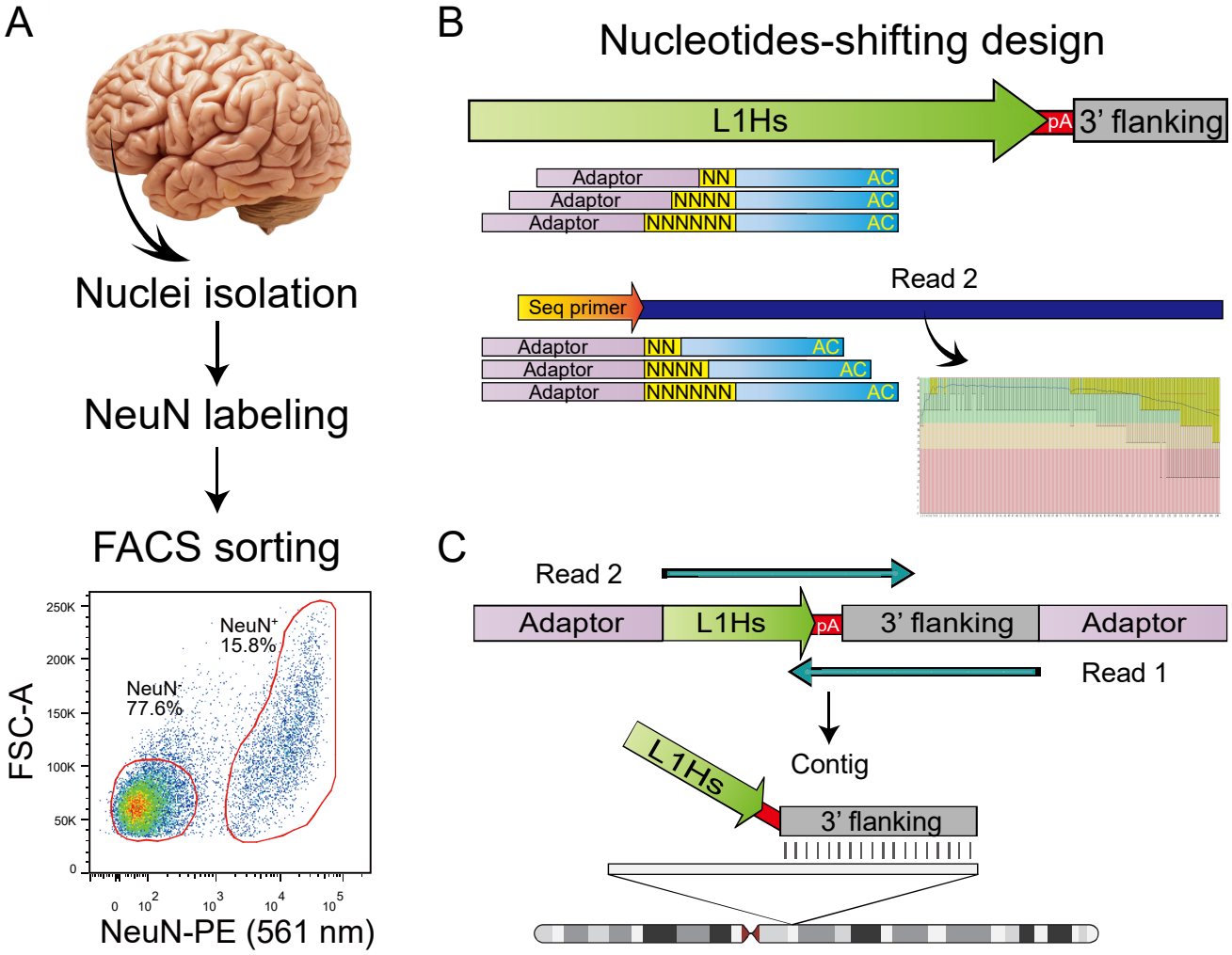

600

601

602 **Fig 1. Overview of human active transposon sequencing (HAT-seq).**

603 (A) Fluorescence-activated cell sorting (FACS) of prefrontal cortex (PFC) nuclei labeled with NeuN.
604 Two populations ($NeuN^+$ and $NeuN^-$) were sorted. (B) Schematic of the nucleotides-shifting design of
605 the HAT-seq method. By adding two, four, or six random nucleotides upstream of L1Hs-specific primer
606 (L1Hs-AC-28), we transformed the library from a uniform phase-0 amplicon library to a mixed library
607 with phase-2, phase-4, and phase-6 amplicons, which remarkedly improved the base calling accuracy
608 in Read 2. (C) HAT-seq libraries were sequenced with paired-end 150-bp reads. After merging paired
609 reads into contigs that fully spanned the L1Hs-genome 3' junction, genomic locations of each L1Hs
610 insertion were determined by the alignments of their 3' flanking genomic sequences.
611

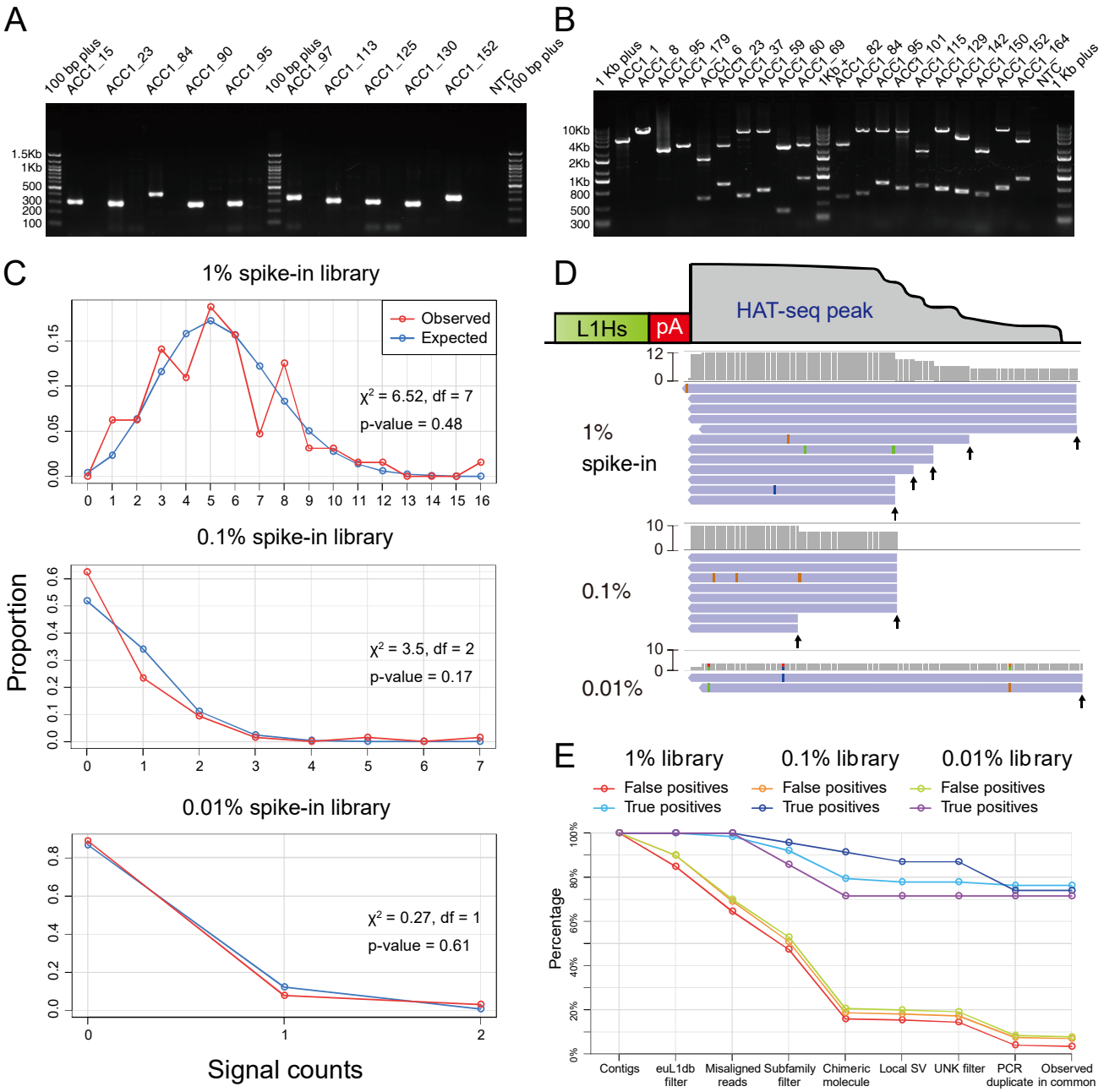
A
100 bp plus
ACC1_15
ACC1_23
ACC1_84
ACC1_90
ACC1_95
100 bp plus
ACC1_97
ACC1_113
ACC1_125
ACC1_130
ACC1_152
NTC
100 bp plus
1.5Kb
1Kb
500
300
200
100
B
1 Kb plus
ACC1_1
ACC1_8
ACC1_95
ACC1_179
ACC1_6
ACC1_23
ACC1_37
ACC1_59
ACC1_60
ACC1_69
1Kb+
ACC1_82
ACC1_84
ACC1_95
ACC1_101
ACC1_115
ACC1_129
ACC1_142
ACC1_150
ACC1_152
ACC1_164
NTC
1 Kb plus
10Kb
4Kb
2Kb
1Kb
800
500
300
C
1% spike-in library
Observed
Expected
χ² = 6.52, df = 7
p-value = 0.48
0.1% spike-in library
χ² = 3.5, df = 2
p-value = 0.17
0.01% spike-in library
χ² = 0.27, df = 1
p-value = 0.61
Proportion
Signal counts
D
L1Hs
pA
HAT-seq peak
1%
spike-in
0.1%
0.01%
E
1% library
0.1% library
0.01% library
False positives
True positives
Percentage
Contigs
euL1db filter
Misaligned reads
Subfamily filter
Chimeric molecule
Local SV
UNK filter
PCR duplicate
Observed in common

614 **Fig 2. HAT-seq performance evaluation using a positive control.**

615 (A) Representative gel image used for the identification of ACC1-specific insertions based on 3' PCR
616 analysis. For each site, genomic DNA from ACC1 and ACC2 was amplified using the same protocol.
617 NTC: negative control. (B) Representative gel image used for the zygosity analysis of ACC1-specific
618 insertions based on full-length PCR. The four sites on the left were homozygous L1Hs insertions and
619 the others were heterozygous L1Hs insertions. (C) The distributions of signal counts (reads with unique
620 start positions) per ACC1-specific insertion closely followed Poisson distributions (chi-squared
621 goodness-of-fit tests). (D) Representative ACC1-specific insertion (ACC1_132 at chr21:29069173) in
622 1%, 0.1%, and 0.01% spike-in libraries. Read coverage and supporting signal counts (unique start
623 positions were indicated by black arrows) were positively correlated with the spike-in concentration.
624 (E) The effectiveness of error filters. 64 ACC1-specific germline insertions in 1%, 0.1%, and 0.01%
625 spike-in libraries were considered as "true positives"; all other signals were considered as "false
626 positives", which might include both background noise and some true somatic insertions present in the
627 blood gDNA.
628

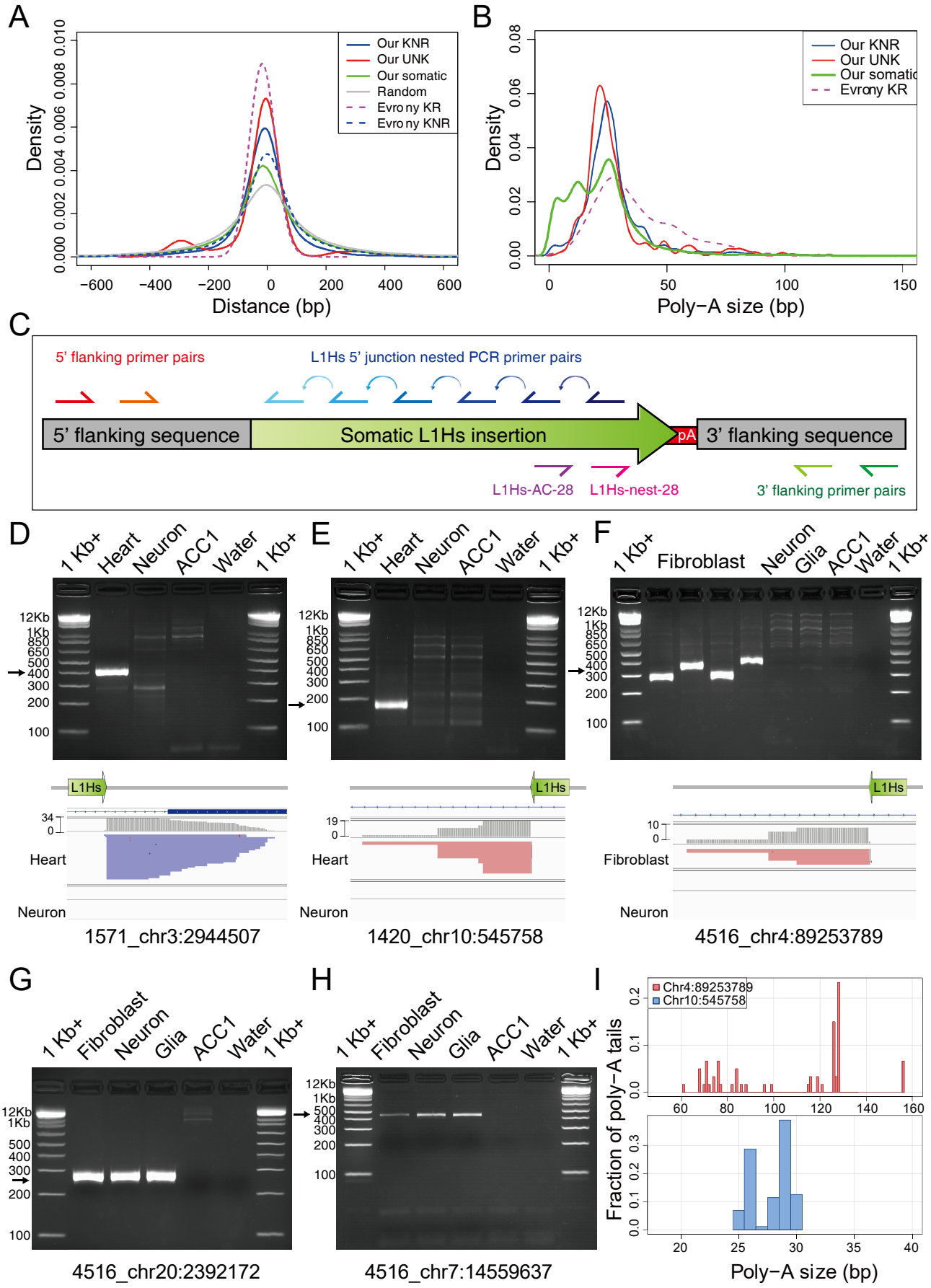
A
Density
Distance (bp)
Our KNR
Our UNK
Our somatic
Random
Evrony KR
Evrony KNR
B
Density
Poly−A size (bp)
Our KNR
Our UNK
Our somatic
Evrony KR
C
5' flanking primer pairs
L1Hs 5' junction nested PCR primer pairs
5' flanking sequence
Somatic L1Hs insertion
pA
3' flanking sequence
L1Hs-AC-28
L1Hs-nest-28
3' flanking primer pairs
D
1 Kb+
Heart
Neuron
ACC1
Water
1 Kb+
12Kb
1Kb
850
650
500
400
300
200
100
L1Hs
Heart
Neuron
1571_chr3:2944507
E
1 Kb+
Heart
Neuron
ACC1
Water
1 Kb+
L1Hs
Heart
Neuron
1420_chr10:545758
F
1 Kb+
Fibroblast
Neuron
Glia
ACC1
Water
1 Kb+
L1Hs
Fibroblast
Neuron
4516_chr4:89253789
G
1 Kb+
Fibroblast
Neuron
Glia
ACC1
Water
1 Kb+
4516_chr20:2392172
H
1 Kb+
Fibroblast
Neuron
Glia
ACC1
Water
1 Kb+
4516_chr7:14559637
I
Chr4:89253789
Chr10:545758
Fraction of poly−A tails
Poly−A size (bp)

629
630

Fig 3. Profiling of somatic L1Hs insertions in multiple human tissues.

(A) The density distributions of L1 EN motifs around L1Hs integration sites. L1 EN motifs included seven specific motifs (TTAAAA, TTAAGA, TTAGAA, TTGAAA, TTAAAG, CTAAAA, TCAAAA). "Evrony KR" and "Evrony KNR" are germline L1Hs insertions identified in Evrony *et al.* 2012. (B) The density distributions of poly-A tail length for each category of L1Hs insertion. (C) The PCR validation scheme and locations of primers used. (D)–(H) Representative gel images of 3' nested PCR validation for putative clonal somatic insertions. The Integrative Genomics Viewer screenshots for (D)–(F) showed the coverage track (gray) and the alignment track (blue for read strand [-]; red for read strand [+]) from HAT-seq data. Black arrows indicated bands with target size. 1Kb +: 1 Kb Plus DNA ladder. (I) Polymorphic poly-A tail sizes of clonal somatic insertions. Top: fibroblast-specific somatic L1Hs insertion at chr4:89253789 from Rett patient UMB#4516. Bottom: heart-specific somatic L1Hs insertion at chr10:545758 from Rett patient UMB#1420.

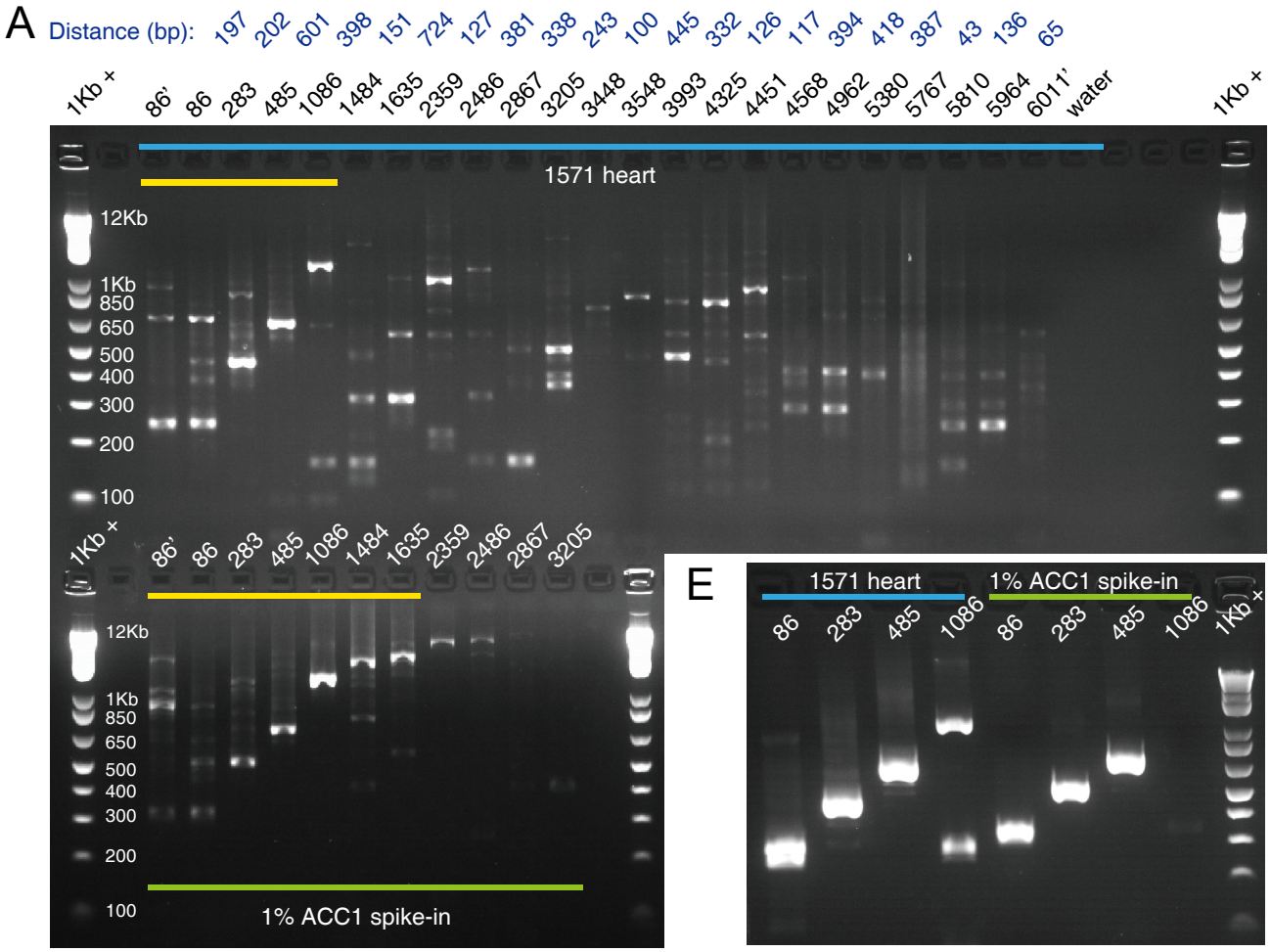
A
Distance (bp): 197 202 601 398 151 724 127 381 338 243 100 445 332 126 117 394 418 387 43 136 65
1Kb + 86' 86 283 485 1086 1484 1635 2359 2486 2867 3205 3448 3548 3993 4325 4451 4568 4962 5380 5767 5810 5964 6011' water 1Kb +
1571 heart
12Kb
1Kb
850
650
500
400
300
200
100
1Kb + 86' 86 283 485 1086 1484 1635 2359 2486 2867 3205
12Kb
1Kb
850
650
500
400
300
200
100
1% ACC1 spike-in
E
1571 heart
1% ACC1 spike-in
86 283 485 1086 86 283 485 1086 1Kb +

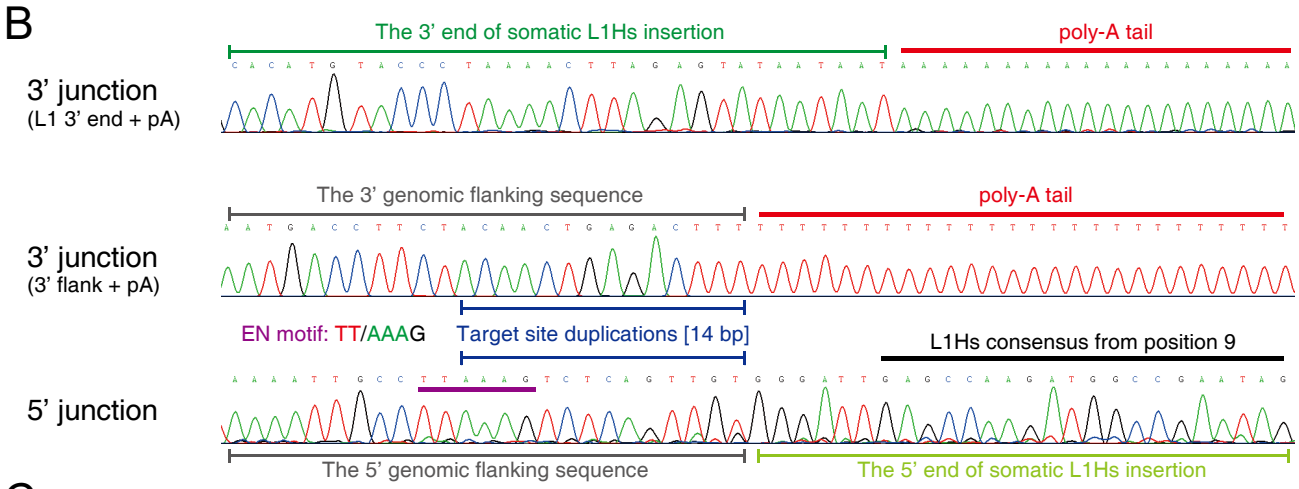
B
The 3' end of somatic L1Hs insertion
poly-A tail
3' junction
(L1 3' end + pA)
The 3' genomic flanking sequence
poly-A tail
3' junction
(3' flank + pA)
EN motif: TT/AAAG
Target site duplications [14 bp]
L1Hs consensus from position 9
5' junction
The 5' genomic flanking sequence
The 5' end of somatic L1Hs insertion

C
Multiple sequence alignment
Species/Abbrv
1. L1Hs
2. L1.3_L19088.1
3. L1.4_L19092.1
4. 1571_chr3:2944507

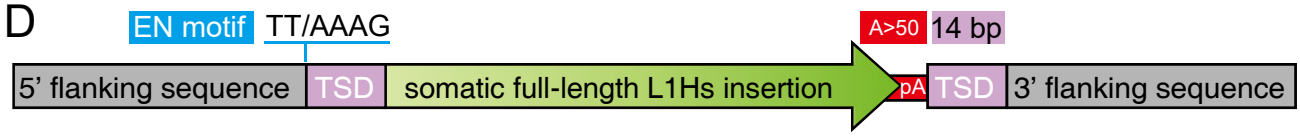
D
EN motif
TT/AAAG
A>50
14 bp
5' flanking sequence
TSD
somatic full-length L1Hs insertion
pA
TSD
3' flanking sequence

Fig 4. A full-length heart-specific L1Hs insertion (1571_chr3:2944507) in a healthy individual. (A) The agarose gel image of 5' junction nested PCR validation for the heart-specific L1Hs insertion in the healthy individual (UMB#1571; upper panel). The locations of primers used in 5' junction PCR assays were labeled on the top of each lane, where primers with the prime symbol denoted semi-nested PCR assays. The distances between each two adjacent 5' step-wise primers were labeled on the top (dark blue). The lower panel represented a heterozygous, full-length L1Hs insertion (ACC1_16; S11 Table and Appendix 4) in 1% ACC1 spike-in gDNA as the positive control. The yellow line highlighted the expected stair-step bands in 5' junction PCR. 1Kb +: 1 Kb Plus DNA ladder. (B) The Sanger sequencing chromatograms of the 3' and 5' junctions of the somatic insertion 1571_chr3:2944507. The L1 EN motif and TSD were indicated by purple and blue lines. (C) Multiple sequence alignment of the 5' end between the identified somatic insertion and three L1Hs consensus sequences (L1Hs Repbase consensus and two hot L1s in human [L1.3 and L1.4]). (D) The schematic structure of 1571_chr3:2944507. (E) The agarose gel image of "full-length PCR + 5' junction PCR" assays for 1571_chr3:2944507 and ACC1_16 positive control.

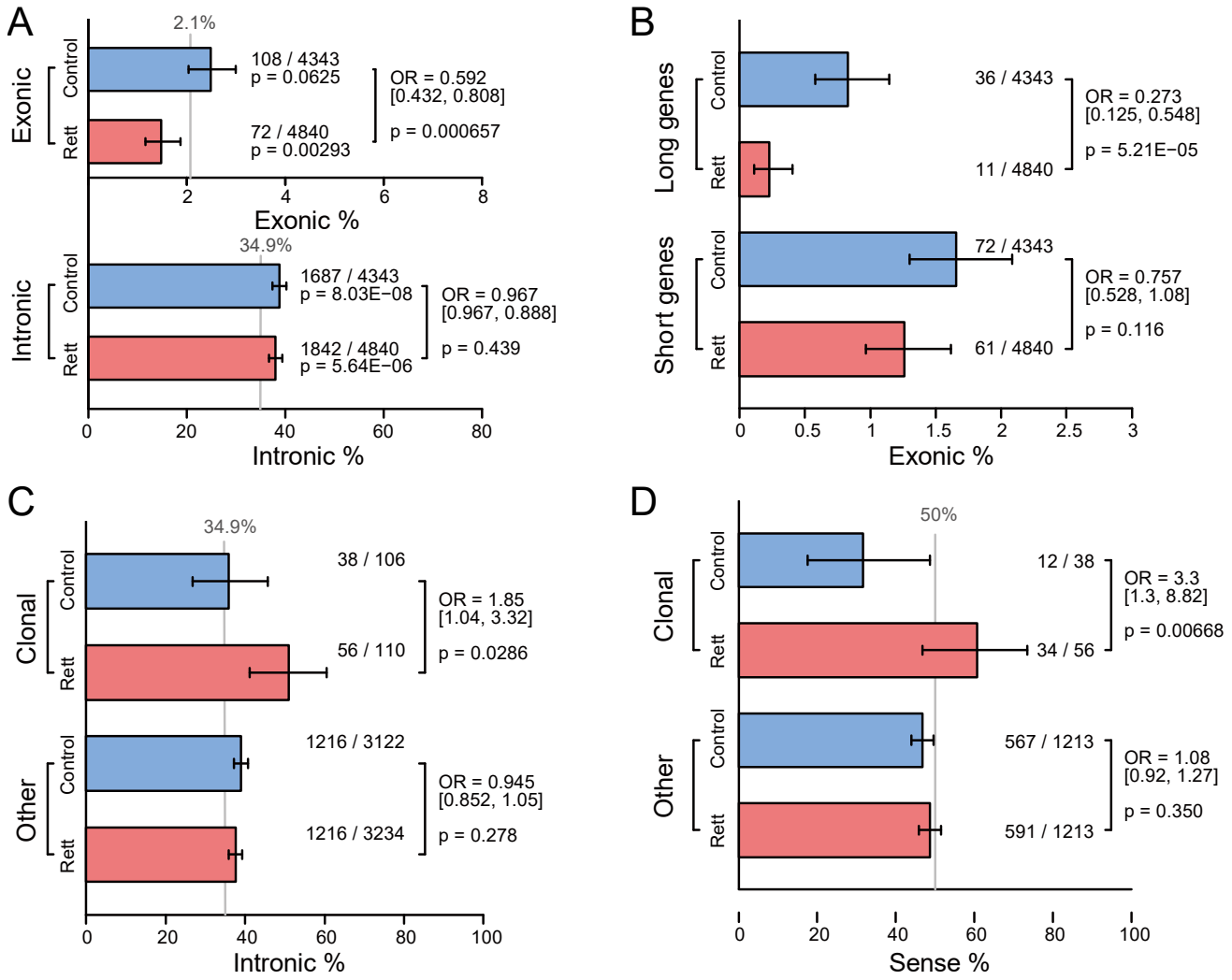
A
Exonic
Control
Rett
2.1%
108 / 4343
p = 0.0625
72 / 4840
p = 0.00293
OR = 0.592
[0.432, 0.808]
p = 0.000657
Exonic %
Intronic
34.9%
1687 / 4343
p = 8.03E−08
1842 / 4840
p = 5.64E−06
OR = 0.967
[0.967, 0.888]
p = 0.439
Intronic %
B
Long genes
36 / 4343
11 / 4840
OR = 0.273
[0.125, 0.548]
p = 5.21E−05
Short genes
72 / 4343
61 / 4840
OR = 0.757
[0.528, 1.08]
p = 0.116
Exonic %
C
Clonal
34.9%
38 / 106
56 / 110
OR = 1.85
[1.04, 3.32]
p = 0.0286
Other
1216 / 3122
1216 / 3234
OR = 0.945
[0.852, 1.05]
p = 0.278
Intronic %
D
Clonal
50%
12 / 38
34 / 56
OR = 3.3
[1.3, 8.82]
p = 0.00668
Other
567 / 1213
591 / 1213
OR = 1.08
[0.92, 1.27]
p = 0.350
Sense %

663 **Fig 5. Abnormal L1Hs mobilization in patients with Rett syndrome.**

664 (A) Percentages of somatic L1Hs insertions in exons and introns. (B) Percentages of somatic L1Hs
665 insertions in exons of long (> 100 kb) and short genes (< 100 kb). (C) Percentages of clonal somatic
666 L1Hs insertions in introns. (D) Percentages of sense-oriented clonal somatic L1Hs insertions. The gray
667 lines in (A) and (C) denoted the expected proportion determined by the exact base-pair count of that
668 specific region relative to the human genome. The gray line in (D) represented the expected proportion
669 if the insertions occurred randomly in both directions. Error bars in (A)–(D) indicated the 95%
670 confidence intervals.

671

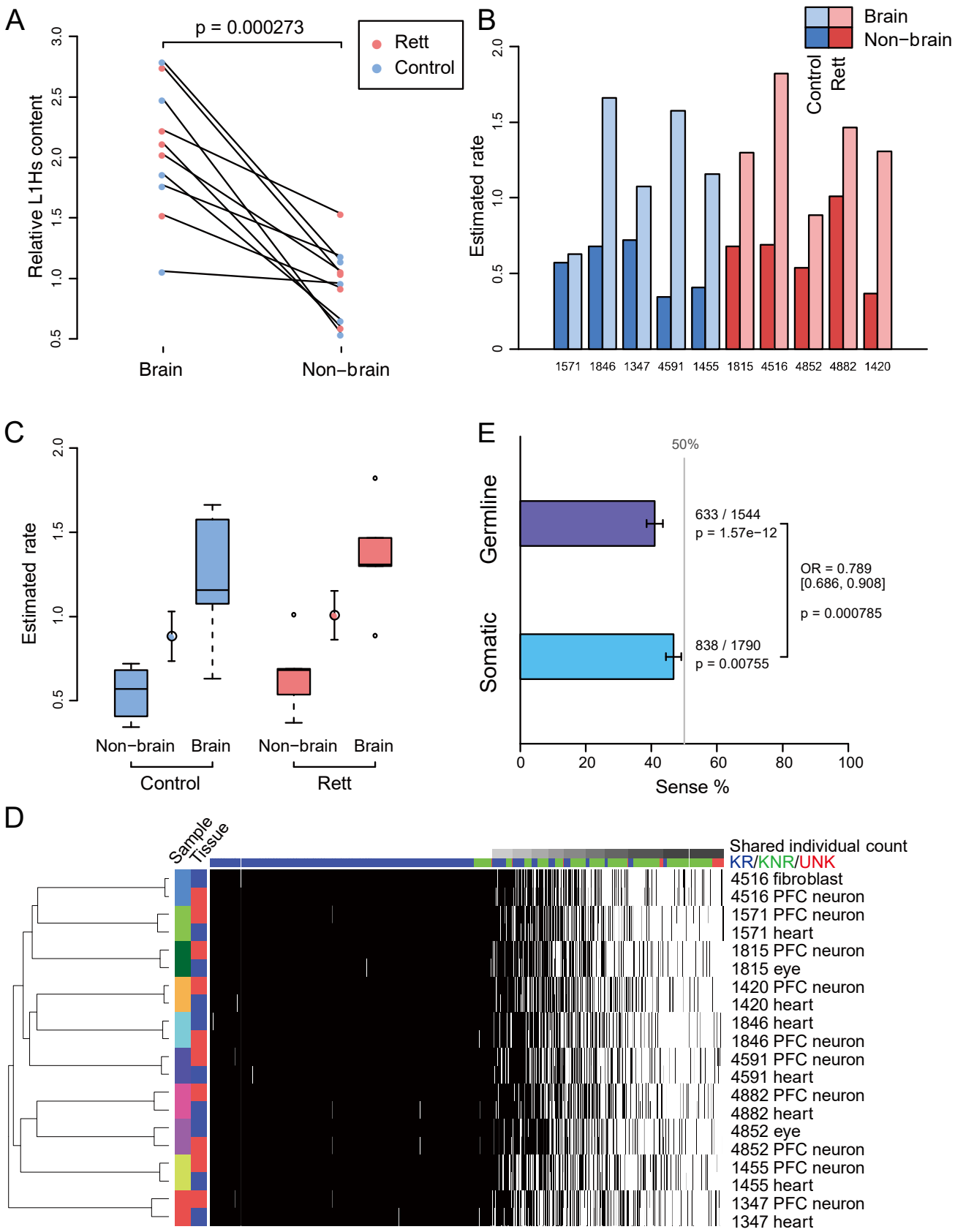
A
p = 0.000273
Rett
Control
Relative L1Hs content
Brain
Non−brain
B
Brain
Non−brain
Control
Rett
Estimated rate
1571 1846 1347 4591 1455 1815 4516 4852 4882 1420
C
Estimated rate
Non−brain Brain Non−brain Brain
Control
Rett
E
50%
Germline
Somatic
633 / 1544
p = 1.57e−12
OR = 0.789
[0.686, 0.908]
p = 0.000785
838 / 1790
p = 0.00755
Sense %
D
Sample
Tissue
Shared individual count
KR/KNR/UNK
4516 fibroblast
4516 PFC neuron
1571 PFC neuron
1571 heart
1815 PFC neuron
1815 eye
1420 PFC neuron
1420 heart
1846 heart
1846 PFC neuron
4591 PFC neuron
4591 heart
4882 PFC neuron
4882 heart
4852 eye
4852 PFC neuron
1455 PFC neuron
1455 heart
1347 PFC neuron
1347 heart

674 **Fig 6. Genome-wide patterns of somatic and germline L1Hs insertions.**

675 (A) Relative somatic L1Hs content in PFC neurons and non-brain tissue from the same donor. The
676 read count ratio of somatic insertions to germline KNR was calculated and then normalized relative to
677 the average value of non-brain samples. The linked dots represented pairs of brain and non-brain
678 samples obtained from the same individual. (B) Histogram of estimated rate of somatic L1Hs insertions
679 in each of tissue samples from the same donor based on the germline KNR copy number of each
680 individual. (C) Estimated rate of somatic L1Hs insertions for different tissue types and cohorts. Error
681 bars denoted the standard error of the mean (S.E.M). (D) Hierarchical clustering of all samples
682 sequenced in this study. Each row represented a sample, and each column represents an L1Hs germline
683 insertion. Black and white squares indicated the presence or absence of insertion, respectively. Column
684 annotations showed categories for known reference (KR; blue), known non-reference (KNR; green),
685 and unknown (UNK; red) insertions. (E) Percentages of sense-oriented germline and somatic L1Hs
686 insertions in transcripts. The gray line represented the expected proportion if the insertions occurred
687 randomly in both directions. Error bars indicated the 95% confidence intervals.
688

Supporting Information

Supplementary Figures

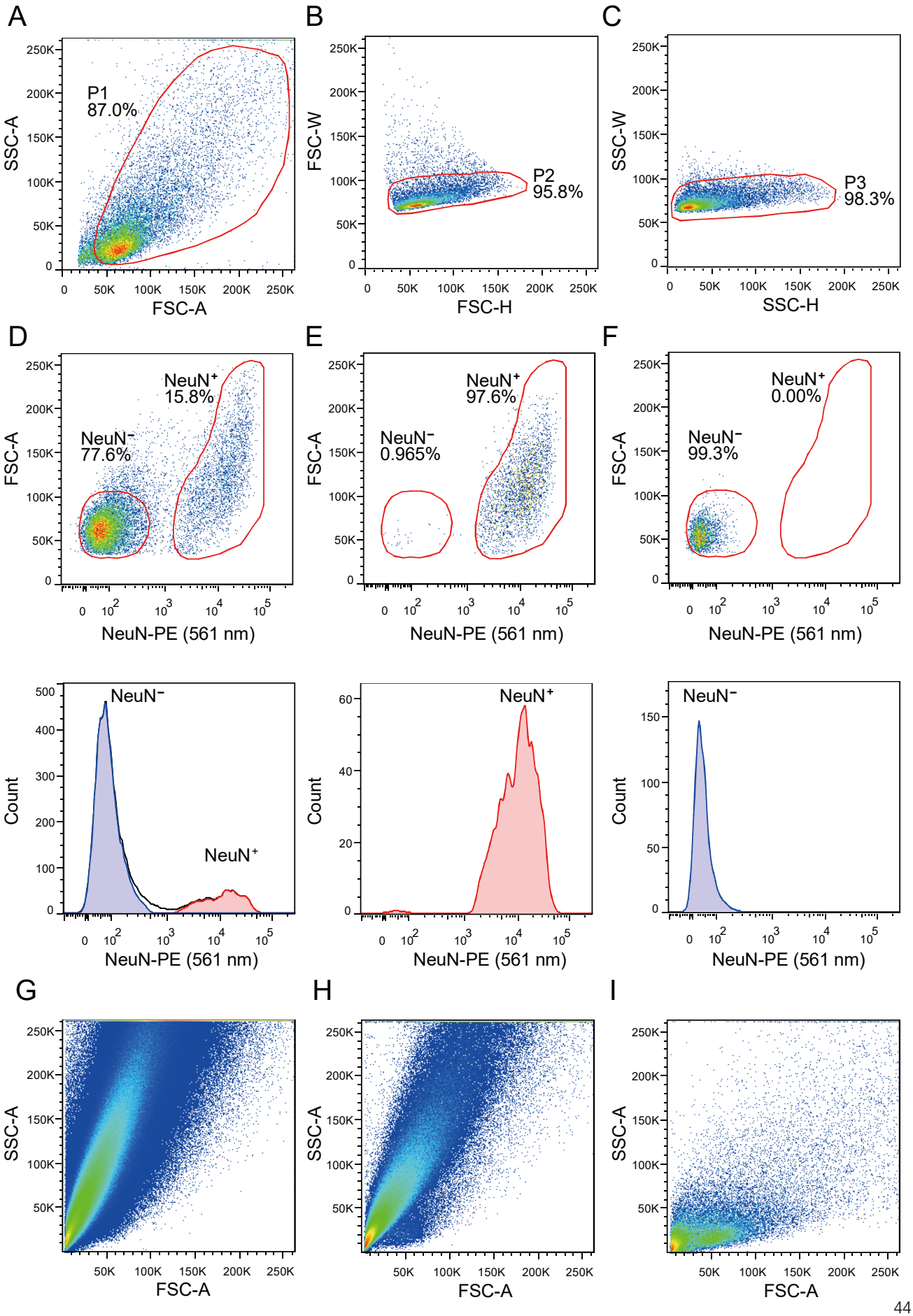
A
P1
87.0%
SSC-A
FSC-A
B
P2
95.8%
FSC-W
FSC-H
C
P3
98.3%
SSC-W
SSC-H
D
NeuN⁺
15.8%
NeuN⁻
77.6%
FSC-A
NeuN-PE (561 nm)
E
NeuN⁺
97.6%
NeuN⁻
0.965%
FSC-A
NeuN-PE (561 nm)
F
NeuN⁺
0.00%
NeuN⁻
99.3%
FSC-A
NeuN-PE (561 nm)
NeuN⁻
NeuN⁺
Count
NeuN-PE (561 nm)
NeuN⁺
Count
NeuN-PE (561 nm)
NeuN⁻
Count
NeuN-PE (561 nm)
G
SSC-A
FSC-A
H
SSC-A
FSC-A
I
SSC-A
FSC-A

691

692 **S1 Fig. Nuclei isolation and NeuN$^+$ fluorescence-activated cell sorting (FACS).**

693 (A)–(D) Purify neuronal nuclei from human PFC. (A) The first gate (P1) was set as an FSC-A vs. SSC-
694 A plot to discriminate the population containing small-size debris. (B)–(C) The second (P2) and third
695 (P3) gates were set as FSC-H vs. FSC-W and SSC-H vs. SSC-D plots, respectively, to remove doublets
696 and clumps. (D) Top: NeuN$^-$ and NeuN$^+$ gates were set in the NeuN-PE (561 nm) vs. FSC-A plot.
697 Bottom: a count plot of NeuN-stained nuclei. (E) Purity analysis of sorted neurons. Top: sorted NeuN$^+$
698 nuclei were re-analyzed by FACS to confirm the sort purity. Bottom: a count plot of re-analyzed NeuN$^+$
699 nuclei. (F) Purity analysis of sorted glia. Top: sorted NeuN$^-$ nuclei were re-analyzed by FACS to
700 confirm the sort purity. Bottom: a count plot of re-analyzed NeuN$^-$ nuclei. (G) FSC vs. SSC plot of
701 brain homogenate. Brain homogenate contained a huge amount of cell debris and myelin debris. (H)
702 FSC vs. SSC plot of debris-detached single-nuclei homogenate. Minced brain tissue was soaked
703 overnight before homogenization and then incubated with nonionic detergent, Nonidet P-40, to remove
704 cell debris from nuclear membrane. (I) FSC vs. SSC plot of debris removed nuclei fraction. Cell debris
705 and myelin were separated from nuclei using Percoll density gradient centrifugation.
706

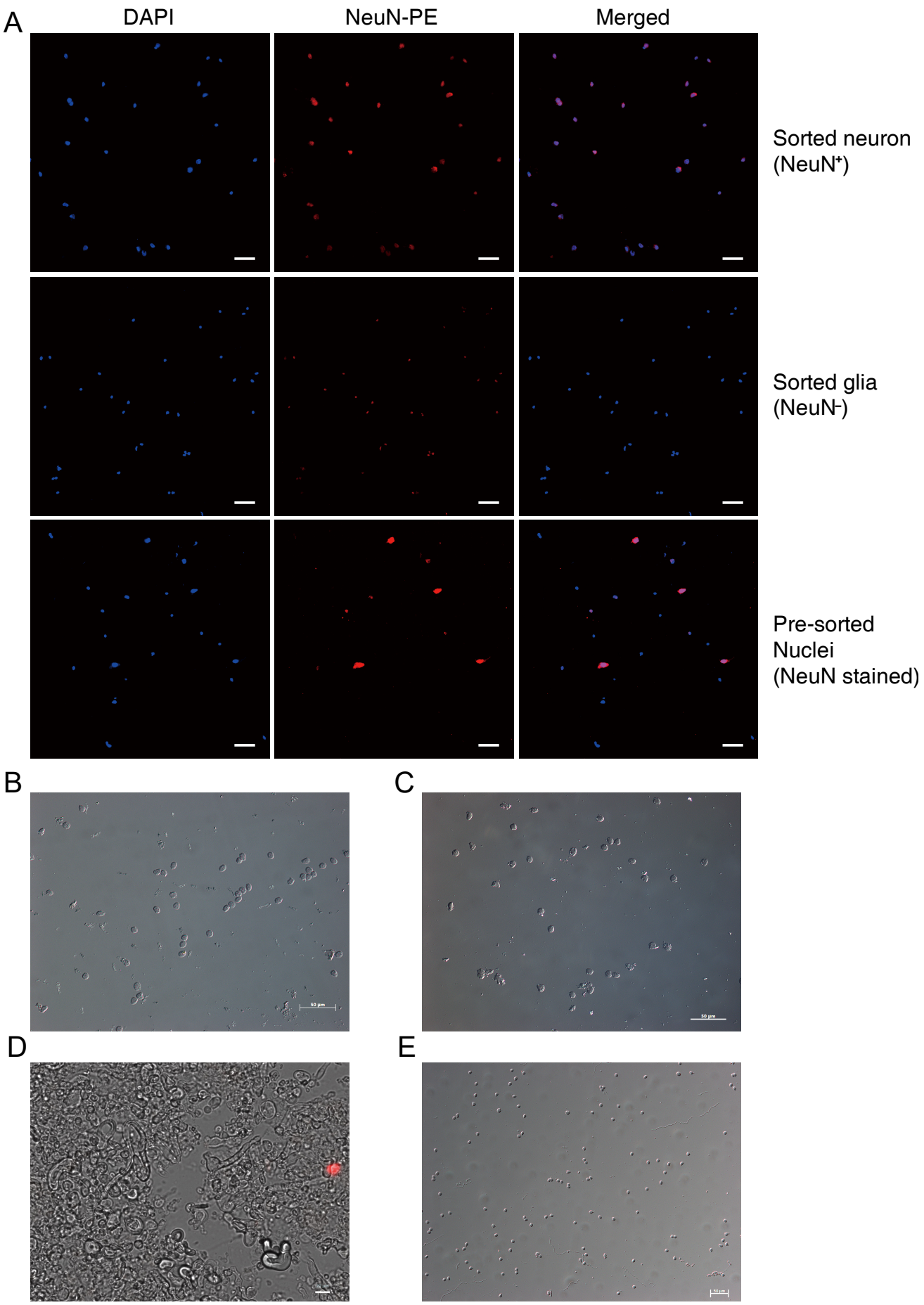
A
DAPI
NeuN-PE
Merged
Sorted neuron
(NeuN+)
Sorted glia
(NeuN-)
Pre-sorted
Nuclei
(NeuN stained)
B
C
D
E

707

S2 Fig. Confirmation of NeuN$^+$ FACS purity and integrity.

(A) Example of fluorescence microscopy confirmation of isolated nuclei. The purity of each fraction was > 95% for NeuN$^+$ and NeuN$^-$ nuclei. Bar = 50 μm. (B)–(C) Examples of integrity confirmation using differential interference contrast (DIC) of sorted neurons (B) and glia (C). Bar = 50 μm. (D) Example of the myelin, lipid, and cell debris layers (12% Percoll) after Percoll density gradient centrifugation. Nuclei were stained with a red fluorescent nuclear counterstain, propidium iodide (PI). Bar = 20 μm. (E) Example of the nuclei fraction layer (35% Percoll) after Percoll density gradient centrifugation. Bar = 50 μm. DAPI, 4',6-diamidino-2-phenylindole; NeuN-PE, PE-conjugated anti-NeuN antibody.

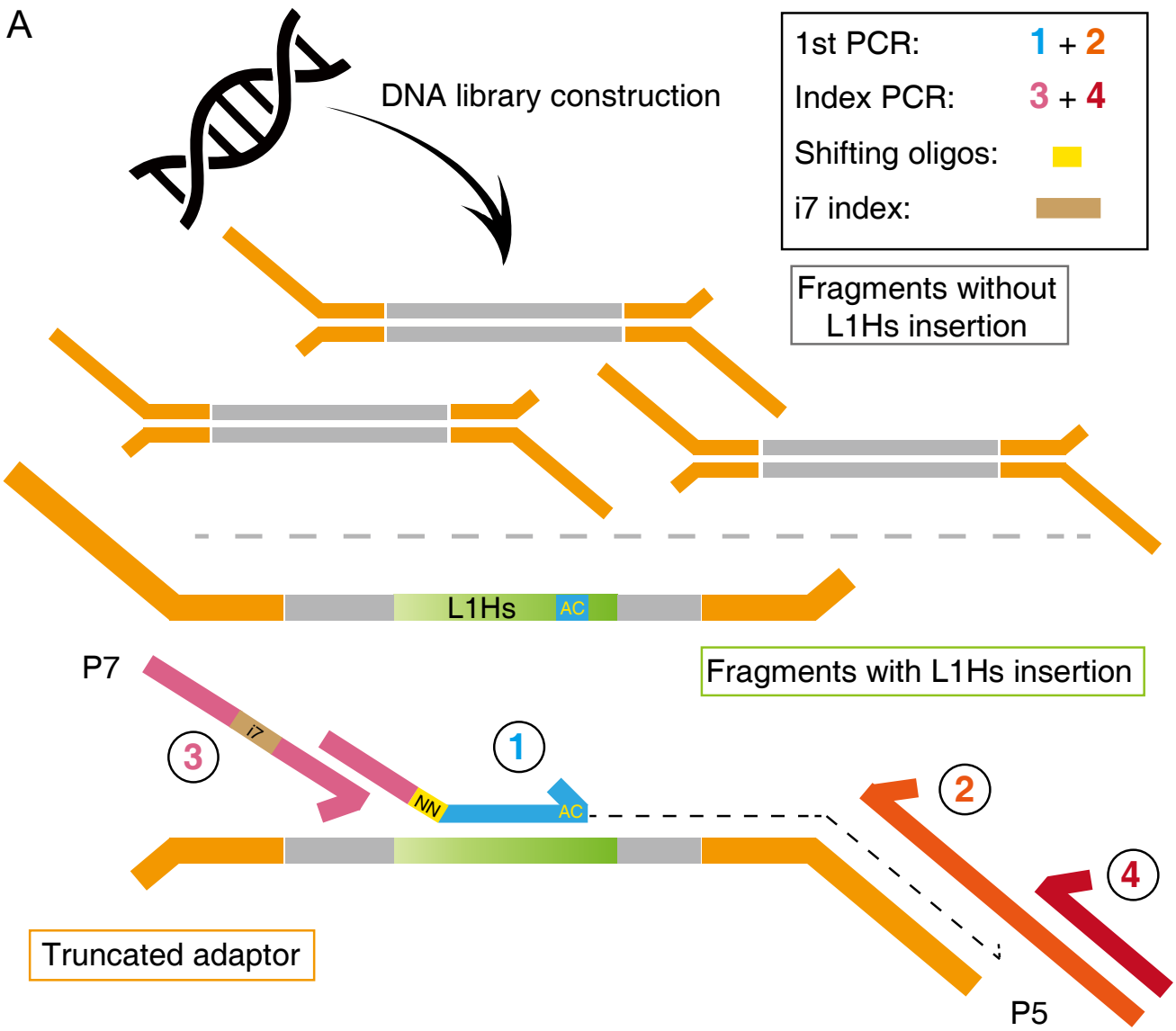
A
DNA library construction
1st PCR: 1 + 2
Index PCR: 3 + 4
Shifting oligos:
i7 index:
Fragments without L1Hs insertion
L1Hs
AC
P7
Fragments with L1Hs insertion
3
i7
1
NN
AC
2
4
Truncated adaptor
P5

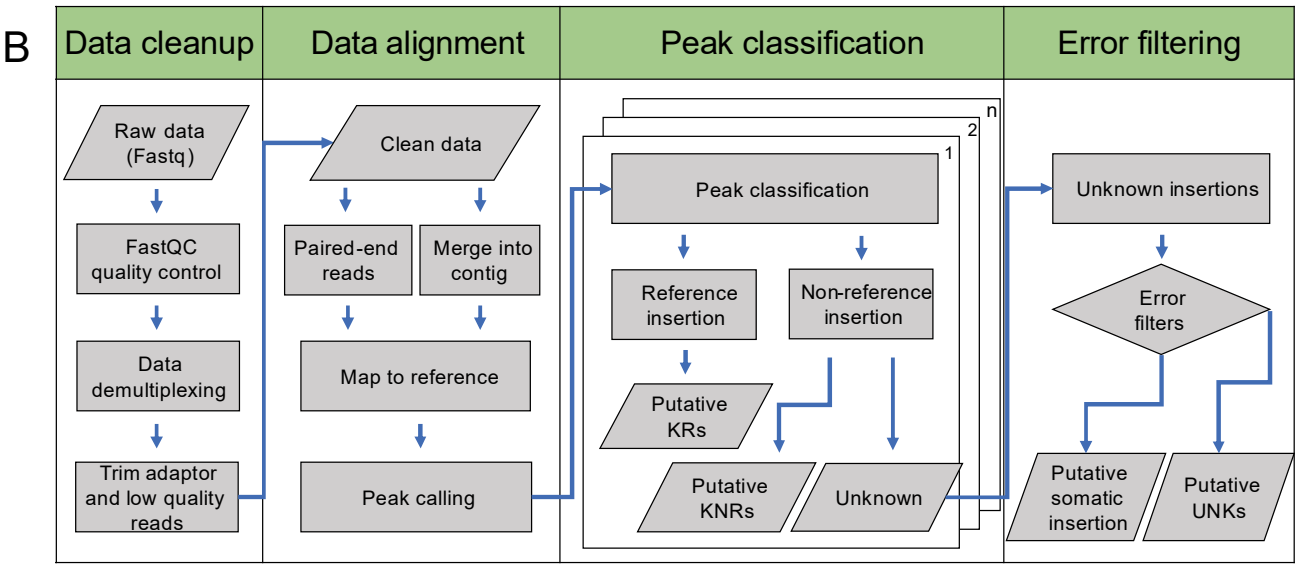
B
Data cleanup
Data alignment
Peak classification
Error filtering
Raw data (Fastq)
FastQC quality control
Data demultiplexing
Trim adaptor and low quality reads
Clean data
Paired-end reads
Merge into contig
Map to reference
Peak calling
n
2
1
Peak classification
Reference insertion
Non-reference insertion
Putative KRs
Putative KNRs
Unknown
Unknown insertions
Error filters
Putative somatic insertion
Putative UNKs

720 **S3 Fig. Schematic diagrams of HAT-seq library construction and computational analysis pipeline.**

721 (A) Schematic of the HAT-seq library construction. The fragmented genomic DNA was ligated with

722 P7 truncated adaptors, and then used as template for L1Hs amplification PCR. Primers 1 (P7_Ns_L1Hs)

723 was specific to L1Hs diagnostic "AC" motif. See S1 Table for primer sequences. (B) Schematic of the

724 HAT-seq data analysis pipeline; full details are provided in the Materials and Methods.

725

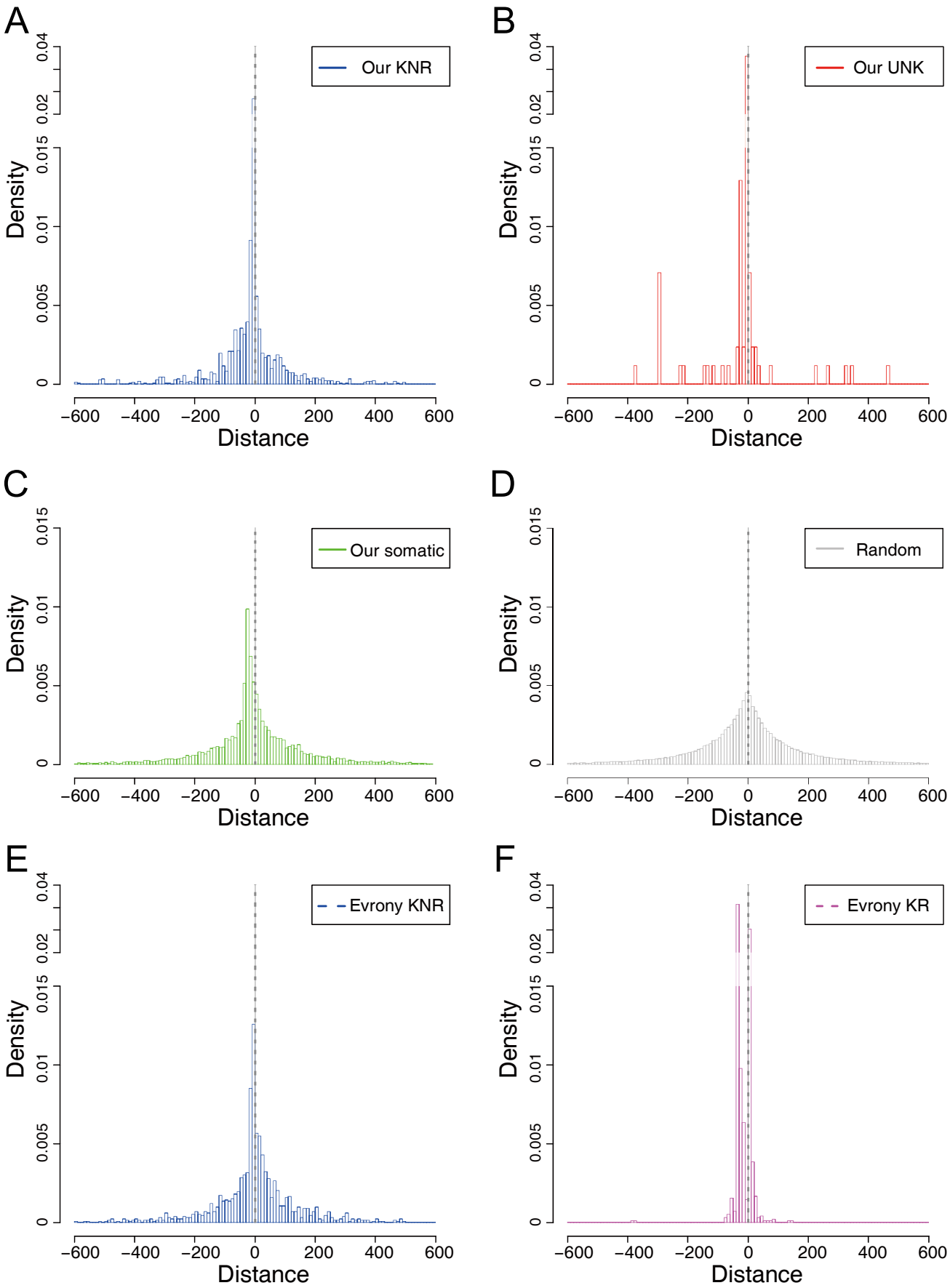
A
Our KNR
Density
Distance
B
Our UNK
Density
Distance
C
Our somatic
Density
Distance
D
Random
Density
Distance
E
Evrony KNR
Density
Distance
F
Evrony KR
Density
Distance

728 **S4 Fig. EN motif enrichment analysis across all categories of L1Hs insertions.**

729 The density distributions of L1 EN motifs around germline KNR (A), UNK (B), somatic insertions
730 (C), randomly sampled positions (D), "Evrony KR" (E), and "Evrony KNR" (F). The lists of "Evrony
731 KR" and "Evrony KNR" were extracted from Evrony *et al.* 2012. The bin size of histogram was 10bp.
732 L1 EN motifs included seven specific motifs (TTAAAA, TTAAGA, TTAGAA, TTGAAA, TTAAAG,
733 CTAAAA, TCAAAA).

734

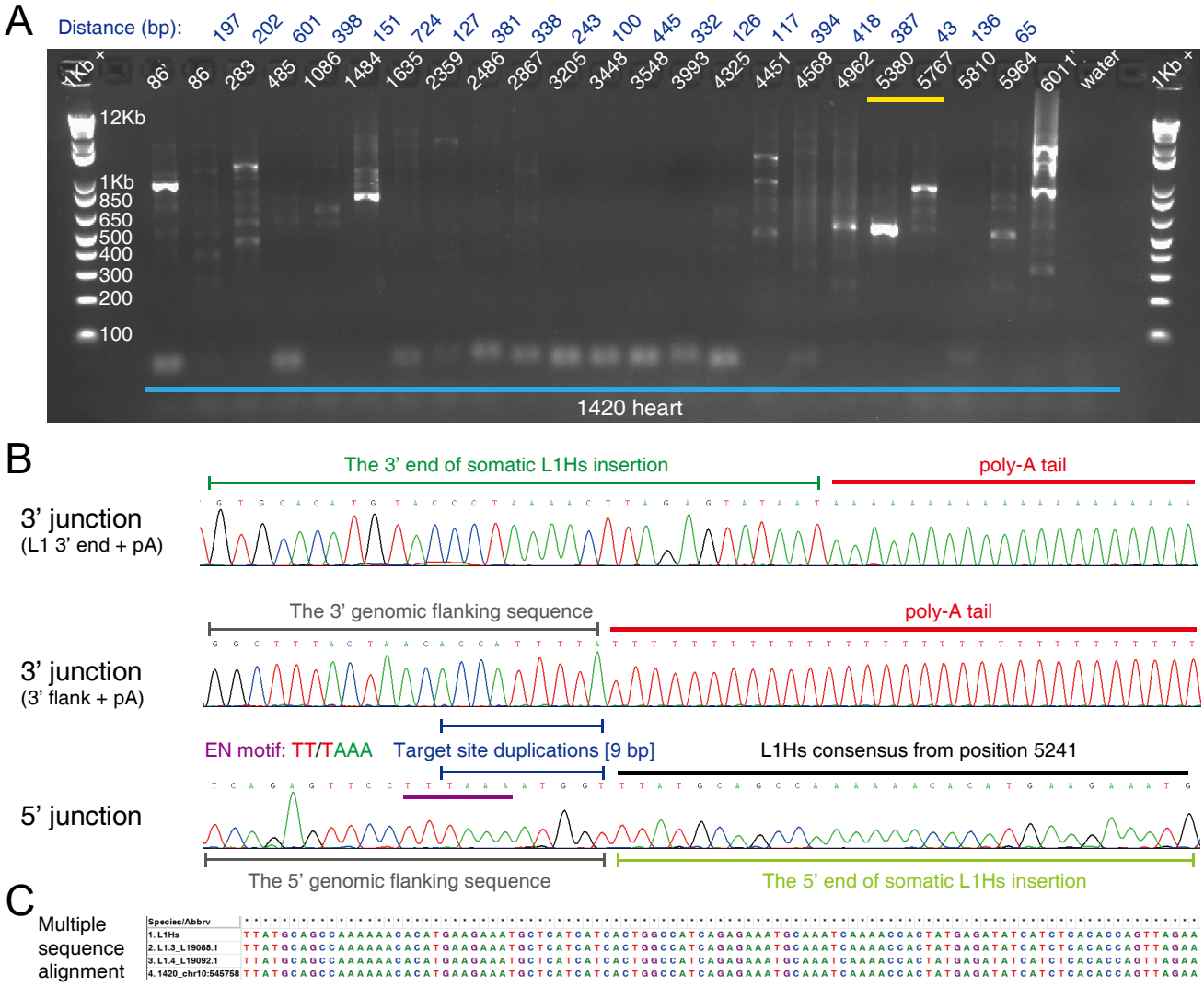
A
Distance (bp): 197 202 601 398 151 724 127 381 338 243 100 445 332 126 117 394 418 387 43 136 65
1Kb + 86' 86 283 485 1086 1484 1635 2359 2486 2867 3205 3448 3548 3993 4325 4451 4568 4962 5380 5767 5810 5964 6011' water 1Kb +
12Kb
1Kb
850
650
500
400
300
200
100
1420 heart
B
The 3' end of somatic L1Hs insertion
poly-A tail
3' junction
(L1 3' end + pA)
The 3' genomic flanking sequence
poly-A tail
3' junction
(3' flank + pA)
EN motif: TT/TAAA
Target site duplications [9 bp]
L1Hs consensus from position 5241
5' junction
The 5' genomic flanking sequence
The 5' end of somatic L1Hs insertion
C
Multiple sequence alignment
Species/Abbrv
1. L1Hs
2. L1.3_L19088.1
3. L1.4_L19092.1
4. 1420_chr10:545758
D
EN motif
TT/TAAA
A>25
9 bp
5' flanking sequence
TSD
5' truncated L1Hs insertion
pA
TSD
3' flanking sequence

S5 Fig. A 5' truncated heart-specific L1Hs insertion (1420_chr10:545758) in a Rett patient. (A) The agarose gel image of 5' junction nested PCR validation for the heart-specific L1Hs insertion in the Rett patient (UMB#1420). The locations of primers used in 5' junction PCR assays were labeled on the top of each lane, where primers with the prime symbol denoted semi-nested PCR assays. The distances between each two adjacent 5' step-wise primers were labeled on the top (dark blue). The yellow line highlighted the expected stair-step bands in 5' junction PCR. 1Kb +: 1 Kb Plus DNA ladder. (B) The Sanger sequencing chromatograms of the 3' and 5' junctions of the somatic insertion (1420_chr10:545758). The L1 EN motif and TSD were indicated by purple and blue lines. (C) Multiple sequence alignment of the 5' end between the identified somatic insertion and three L1Hs consensus sequences (L1Hs Repbase consensus and two hot L1s in human [L1.3 and L1.4]). (D) The schematic structure of the highly 5' truncated (~800 bp) L1Hs insertion 1420_chr10:545758.

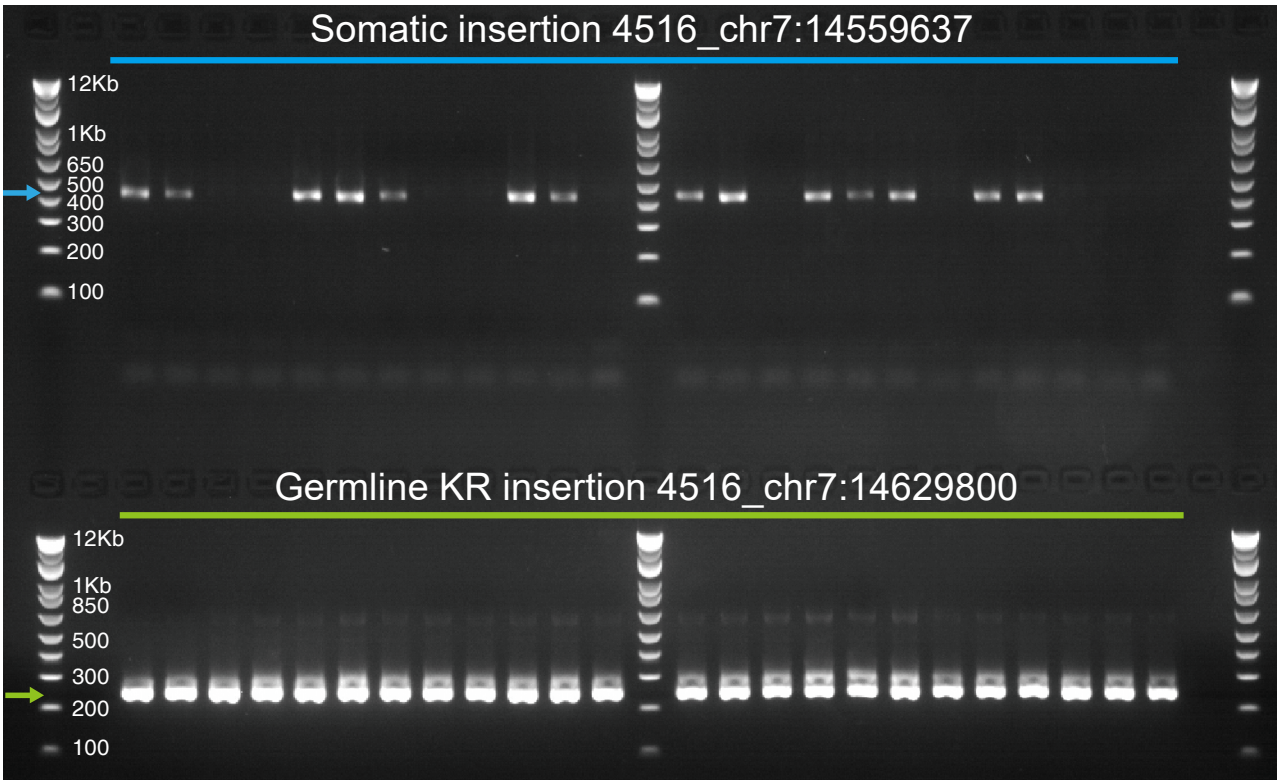
Somatic insertion 4516_chr7:14559637
12Kb
1Kb
650
500
400
300
200
100
Germline KR insertion 4516_chr7:14629800
12Kb
1Kb
850
500
300
200
100

751 **S6 Fig. The somatic status of an L1Hs insertions (4516_chr7:14559637) in a Rett patient.**

752 The somatic insertion 4516_chr7:14559637 was present in 14 out of 24 nested 3' PCR wells, compared

753 to 24 out of 24 wells for a germline KR insertion (chr7:14629800) from the same donor. DNA sample

754 was diluted to ~300 cells per well. Blue and green arrows indicated bands with target size.

755

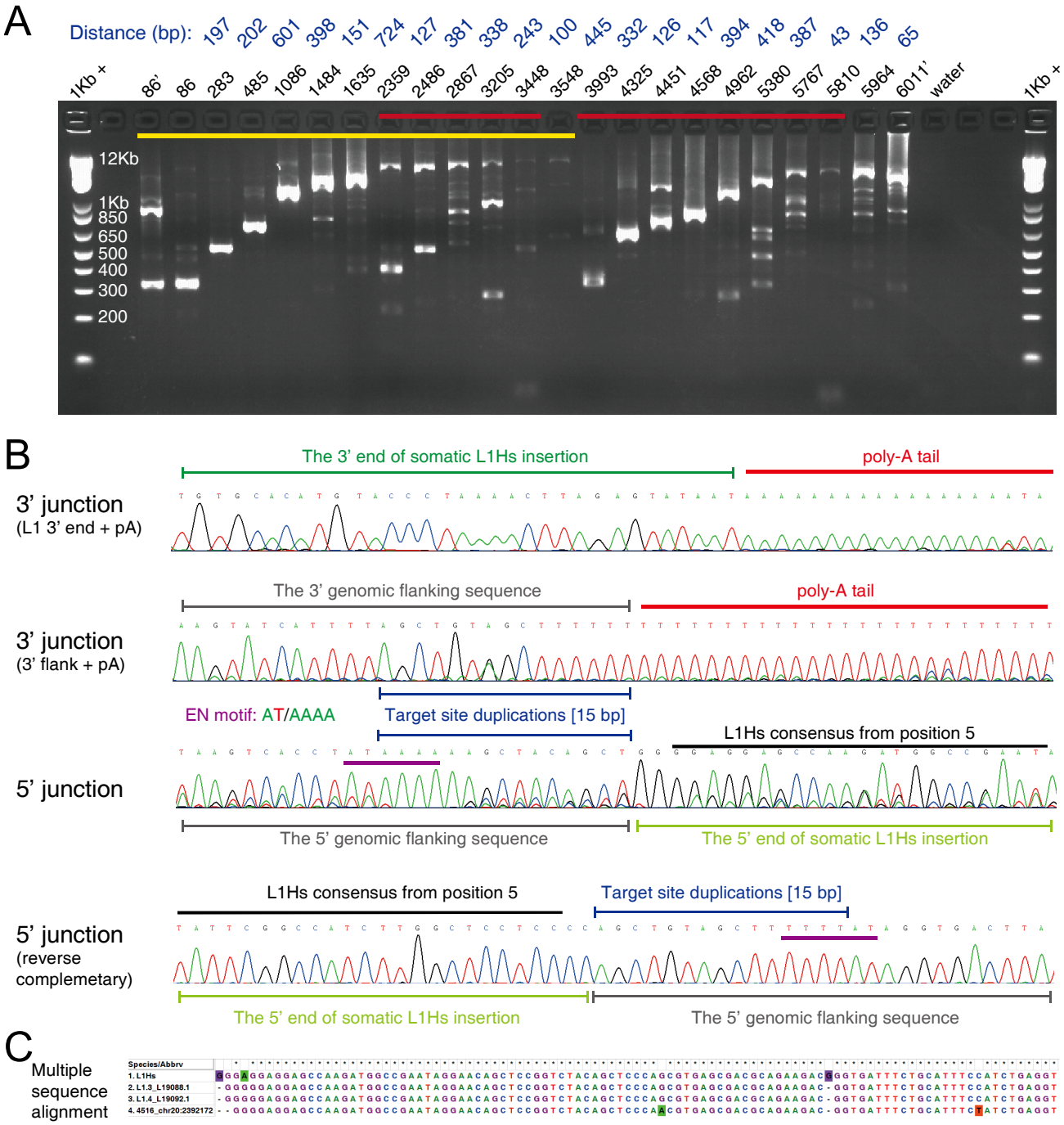
A
Distance (bp): 197 202 601 398 151 724 127 381 338 243 100 445 332 126 117 394 418 387 43 136 65
1Kb + 86' 86 283 485 1086 1484 1635 2359 2486 2867 3205 3448 3548 3993 4325 4451 4568 4962 5380 5767 5810 5964 6011' water 1Kb +
12Kb
1Kb
850
650
500
400
300
200
B
The 3' end of somatic L1Hs insertion
poly-A tail
3' junction
(L1 3' end + pA)
The 3' genomic flanking sequence
poly-A tail
3' junction
(3' flank + pA)
EN motif: AT/AAAA
Target site duplications [15 bp]
L1Hs consensus from position 5
5' junction
The 5' genomic flanking sequence
The 5' end of somatic L1Hs insertion
L1Hs consensus from position 5
Target site duplications [15 bp]
5' junction
(reverse
complemetary)
The 5' end of somatic L1Hs insertion
The 5' genomic flanking sequence
C
Multiple
sequence
alignment
Species/Abbrv
1. L1Hs
2. L1.3_L19088.1
3. L1.4_L19092.1
4. 4516_chr20:2392172
D
EN motif
AT/AAAA
A>40
15 bp
5' flanking sequence
TSD
somatic full-length L1Hs insertion
pA
TSD
3' flanking sequence

S7 Fig. A full-length embryonic somatic L1Hs insertion (4516_chr20:2392172) in a Rett patient. (A) The agarose gel image of 5' junction nested PCR validation for the embryonic somatic L1Hs insertion (4516_chr20:2392172) in the Rett patient (UMB#4516). The locations of primers used in 5' junction PCR assays were labeled on the top of each lane. Step-wise primers with the prime symbol were used twice in semi-nested PCR assays. The distances between each primer pairs were labeled on the top (dark blue). The yellow line highlighted the expected stair-step bands in 5' junction PCR, while the red lines indicated false positives resulted from non-specific amplification of L1PA subfamilies. 1Kb +: 1 Kb Plus DNA ladder. (B) The Sanger sequencing chromatograms of the 3' and 5' junctions of somatic insertion (4516_chr20:2392172). The nucleotides shifted chromatogram in 5' junction might result from the DNA polymerase slippage at homopolymers in the upstream region (L1MB3 element), and its sequence was confirmed from the reverse direction. The L1 EN motif and TSD were indicated by purple and blue lines. (C) Multiple sequence alignment of the 5' end between the identified somatic insertion and three L1Hs consensus sequences (L1Hs Repbase consensus and two hot L1s in human [L1.3 and L1.4]). (D) The schematic structure of 4516_chr20:2392172.

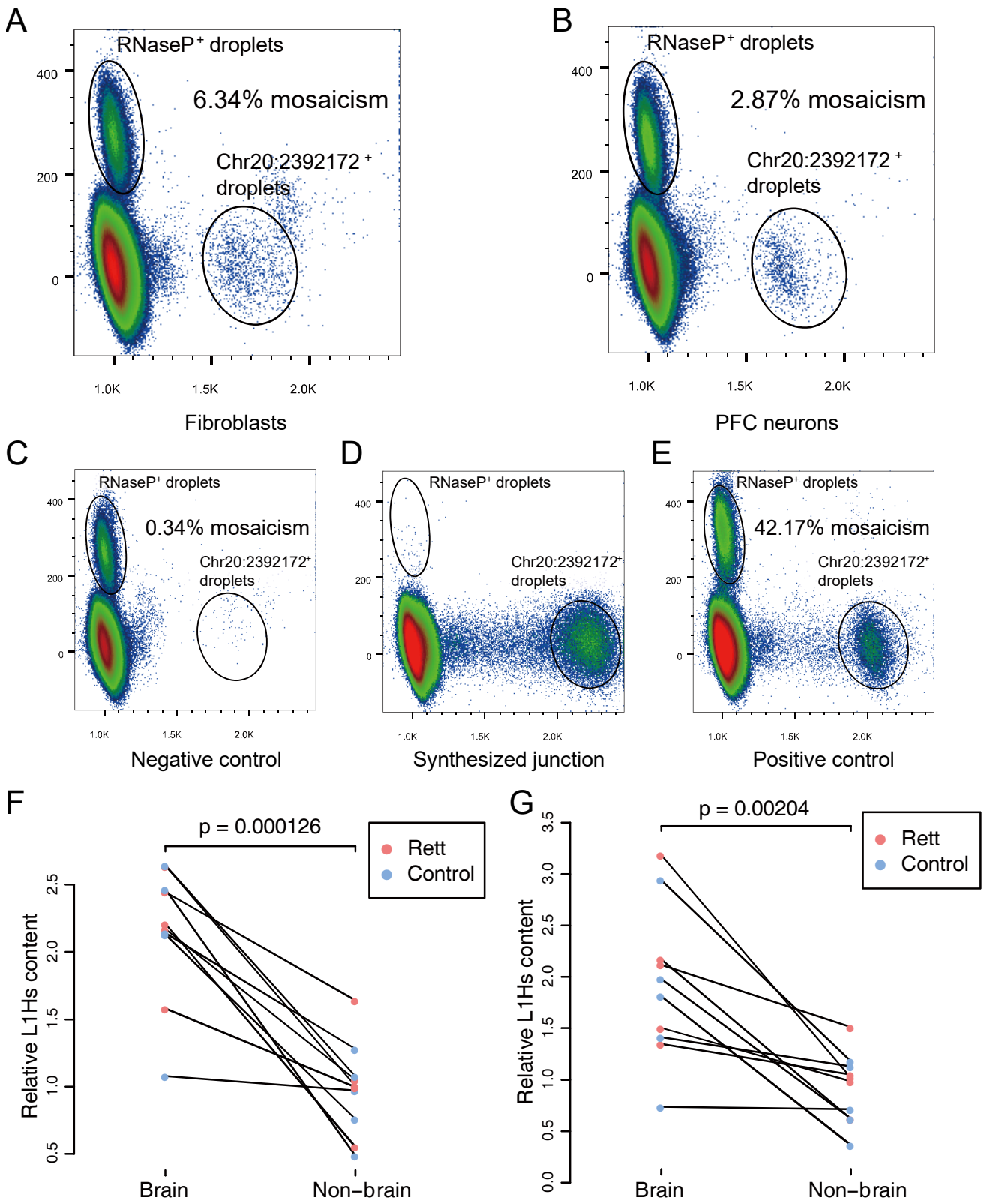
A
RNaseP⁺ droplets
6.34% mosaicism
Chr20:2392172⁺ droplets
Fibroblasts
B
RNaseP⁺ droplets
2.87% mosaicism
Chr20:2392172⁺ droplets
PFC neurons
C
RNaseP⁺ droplets
0.34% mosaicism
Chr20:2392172⁺ droplets
Negative control
D
RNaseP⁺ droplets
Chr20:2392172⁺ droplets
Synthesized junction
E
RNaseP⁺ droplets
42.17% mosaicism
Chr20:2392172⁺ droplets
Positive control
F
p = 0.000126
Rett
Control
Relative L1Hs content
Brain
Non−brain
G
p = 0.00204
Rett
Control
Relative L1Hs content
Brain
Non−brain

775 **S8 Fig. Qualitative and quantitative analysis of L1Hs insertions.**

776 (A)–(E) Droplet digital PCR (ddPCR) assays to quantify mosaicism (percentage of cells) of somatic
777 L1Hs insertions at chr20:2392172 in fibroblasts (A) and PFC neurons (B) from Rett patient
778 UMB#4516. Fragmented ACC1 blood gDNA was used as template for negative control assay (C). A
779 mixed template containing fragmented ACC1 blood gDNA and diluted synthesized L1Hs genome
780 junction oligos (D) was used for positive control assay (E). RNaseP served as a genomic copy number
781 reference (copy number = 2). L1Hs and RNaseP assays were labeled with FAM and VIC, respectively.
782 (F)–(G) Relative somatic L1Hs content in PFC neurons and non-brain tissue from the same donor,
783 normalized by the read count of KRs (F) or UNKs (G) from the same tissue sample.
784

785 **Supplementary Tables**

786

787 **S1 Table. Primer sequences of HAT-seq library**

788

789 **S2 Table. ACC1-specific insertions in positive control experiments**

790

791 **S3 Table. Statistics of error filters in positive control experiments**

792

793 **S4 Table. Clinical characterization of patients with Rett syndrome**

794

795 **S5 Table. Statistics of HAT-seq libraries**

796

797 **S6 Table. Statistics of known reference insertions among all samples**

798

799 **S7 Table. Statistics of polymorphic insertions among all samples**

800

801 **S8 Table. Statistics of somatic insertions among all samples**

802

803 **S9 Table. TPRT hallmark annotation for all somatic insertions**

804

805 **S10 Table. 3' junction nested PCR and digital droplet PCR validation**

806

807 **S11 Table. 5' junction nested PCR validation**

808

809 **S12 Table. Annotation for somatic exonic insertions**

810

811 **S13 Table. Raw data for statistical analyses**

812

813 **S14 Table. Quantification statistics among all samples**

814

815 **S15 Table. L1Hs enrichment analysis on HAT-seq**

816

817 **S16 Table. 3' junction PCR validation for germline insertions**

818

819 **Supplementary Files**

820

821 **Appendix 1. Cell type-specific sorting for postmortem human brain samples**

822

823 **Appendix 2. Identification of ACC1-specific insertions and their zygosity**

824

825 **Appendix 3. Detection of somatic insertions in positive control experiments**

826

827 **Appendix 4. Benchmarking PCR validation assays for low-frequency somatic insertions**

828

829 **Appendix 5. Experimental validation of polymorphic germline L1Hs insertions**